L-Cysteine-Capped Indium Telluriselenide Quantum Dot Aptasensor for Interferon-Gamma TB Biomarker

UNIVERSITY *of the*
WESTERN CAPE

By

Kaylin Cleo Januarie

(BSc Honours)

A mini-thesis submitted in partial fulfilment of the requirements for the degree

Of

Magister Scientiae in Nanoscience

Faculty of Science

University of the Western Cape

Cape Town, South Africa

Supervisor: Prof Emmanuel Iwuoha

January 2018

Abstract

Tuberculosis (TB) is one of the major infectious diseases that affect the health of people all over the world. South Africa is one of the countries that account for most of the TB cases; it is the leading cause of death in South Africa and is known to be lethal when combined with HIV in patients. Various tests have been used to diagnose tuberculosis infected patients, but some of these tests give false positive results. Studies have shown that tuberculosis-related cytokines can serve as biological markers for the diagnosis of TB. Cytokines are signalling proteins secreted by immune cells and one such cytokine is interferon-gamma (IFN-γ). Interferon-gamma is secreted by immune cells in response to various pathogens and has many physiological roles in the immune system and inflammatory stimuli. IFN-γ was first detected using antibody-based immunosensing techniques but this approach is expensive, time consuming and has low stability, it is therefore vital that an alternative detection method for IFN-γ be developed. Hence this study is aimed at developing a fast, simple and sensitive QD based electrochemical aptasensor for the detection of interferon-gamma. In this study L-cysteine capped indium telluriselenide (In_3TeSe_2) quantum dot was produced by microwave synthesis and deposited on gold electrode. The In_3TeSe_2 QD-modified electrode was converted to an IFN-γ aptasensor by the functionalization of the electrode surface with 5'-/Biosg/GCC TGT TGT GAG CCT CCT AAC CTT TAT GAC GGT CTA TAC GCT CTG GTG CAA TTG biotinylated DNA aptamer. The optical properties of the QD was determined by UV-vis and fluorescence (FL) spectrometries which gave an absorbance bands at 291 nm and emission band at 320 nm. The structure of the QD was verified by Fourier transform infrared spectroscopy (FTIR), high resolution transmission electron microscopy (HRTEM), high resolution scanning electron microscopy (HRSEM) and small angle X-ray scattering (SAXS); HRTEM and SAXS results revealed that the quantum dot was spherical in shape, aggregated

and has a diameter of 6 nm. Electro-analysis of the L-cysteine-In_3TeSe_2 QD was done by Cyclic Voltammetry (CV) and Electrochemical Impedance Spectroscopy (EIS). Interferon-gamma was successfully detected using the probe (AuE/L-cysteine-In_3TeSe_2 QD/Aptamer) in PBS buffer solution, pH 7.4. The response parameters of the quantum dot aptasensor to different concentrations of interferon-gamma was studied by cyclic voltammetry (CV), square wave voltammetry (SWV) and electrochemical impedance spectroscopy (EIS). It was observed that all three techniques showed good linearity, with R^2 corresponding to 0.99, however it was perceived that EIS was the best technique for the detection of IFN-γ compared to CV and SWV, since it showed a higher sensitivity (2.25 Ω/pg/mL) and a wide linear range 0.25-1.25 pg/mL.

Declaration

I declare that ***L-cysteine-capped Indium telluriselenide quantum dot aptasensor for Interferon-gamma TB biomarker*** is my own work and has not been submitted before for any degree or examination in any other university, and that all sources I have used or quoted have been indicated and acknowledged as complete references.

Kaylin Januarie Year: 2018

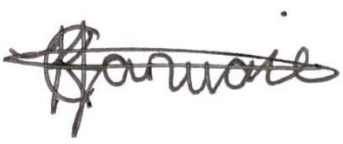

Signed:……..

Acknowledgement

First and foremost I would like to thank the Lord above for giving me the necessary wisdom, insight, patience, strength and understanding to complete this project to the best of my ability, all the honour and glory to you God.

To my mother who is my rock, I cannot begin to describe how much you mean to me and how much your support has helped me throughout this study, I am so blessed to have a God fearing mother like you that loves and motivates me. Thank you for all the sacrifices you have made for me, I would not be where I am today if it wasn't for you, and I owe all my success to you and the Lord above.

To my Supervisor: Prof Emmanuel Iwouha, thank you for your support, encouragement and guidance throughout this study. It has been an honour to be supervised by such a great man.

To the department of chemistry staff and all Sensorlab colleagues especially to Dr Lindsay Wilson and Dr Masikini Milua, thank you for the assistance, guidance, encouragement and knowledge you have given me.

To the Electron Microscope Unit (EMU) at the Physics Department (University of the Western Cape) especially Earl and Natasha, thank you for your assistance with the HRTEM and HRSEM.

To all my friends I have not mentioned thank you for your loving friendship, support and encouragement you have shown me.

I would also like to thank the Nanoscience and Nanotechnology Post Graduate Teaching and Training Platform (NNPTTP) and the Department of Science and Technology for awarding me an MSc Nanoscience Scholarship.

Dedication

I would like to dedicate this work to my loving mother Minnie Januarie.

List of Abbreviations

QD	Quantum dot
TB	Tuberculosis
IFN-γ	Interferon-gamma
In_3TeSe_2	Indium Telluriselenide
L-cys	L-cysteine
PBS	Phosphate Buffer Solution
EDC	1-Ethyl-3-(3-Dimethylaminopropyl) Carbodiimide Hydrochloride
NHS	N-Hydroxysuccinimide
MCH	6-Mercapto-1-Hexanol
AuE	Gold Electrode
UV-vis	Ultraviolet-Visible Spectroscopy
FL	Fluorescence Spectroscopy
FTIR	Fourier Transform Infrared Spectroscopy
SAXS	Small Angle X-ray Scattering
HRSEM	High Resolution Scanning Electron Microscopy
HRTEM	High Resolution Transmission Electron Microscopy
CV	Cyclic Voltammetry
SWV	Square Wave Voltammetry
EIS	Electrochemical Impedance Spectroscopy
R_{ct}	Charge Transfer Resistance
$I_{p,a}$	Anodic Peak Current

Table of Contents

List of Figures

List of Tables

Chapter 1

1.1. Background and Introduction

Tuberculosis (TB) is considered to be a lethal and common disease that is considered to be one of the main health problems around the world. It is caused by (M. tuberculosis) bacteria (Farid, et al., 2015) which usually affects the patient's lungs. Tuberculosis is the second leading infectious disease cause of death worldwide after the human immunodeficiency virus (HIV) (Torati, Reddy, Yoon, & Kim, 2016). There were 8.7 million new cases of active tuberculosis globally, 13% of those involved coinfection with the immunodeficiency virus and there were 1.4 million deaths including 430 000 deaths among HIV-infected patients in 2011 (Zumla, Raviglione, Hafner, & Fordham van Reyn, 2013). Annually people infected with tuberculosis led to the death of 3 million people worldwide because theoretically one tuberculosis patient can transfer the infection to at least 10-20 people in his surroundings (Nurmalasari, Yohan, Gaffar, & Hartati, 2015). Tuberculosis is a contagious disease and is transmitted through aerosols, generated by infected droplets shed through coughing of patients with active pulmonary TB (Parida & Kaufmann, 2010). When a person becomes infected it weakens the immune system and can activate the development of active M. tuberculosis (Nurmalasari, Yohan, Gaffar, & Hartati, 2015). Various tests have been done to diagnose tuberculosis, one of them are the M.tuberculosis direct test (MTD) and the results are then analysed using PCR amplification for M.tuberculosis-specific DNA fragments, the limitations of this test is significant, one of them being that they give false-positive results. Another standard test is the smear sputum microscopy test; however it is unable to identify half of the positive TB infections (Torres-Chavolla & Alocilja, 2011). It has been reported that some tuberculosis related cytokines may be biological markers for the diagnosis of tuberculosis (Min, Cho, Han, Shim, Ku, & Ban, 2008). Cytokines such as interferon-gamma

(IFN-γ) are signalling proteins that is secreted by immune cells, in order to regulate the immune response, regenerate tissues and wound healing process (Farid, et al., 2015). Interferon-gamma possesses antiviral, antiproliferative, differentiation inducing and immuno-regulatory properties. Interferon-gamma is produced by T-helper cells and cytotoxic T-cells. For this reason, detection and quantification of interferon-gamma is important for understanding what immune cells are partaking in the immune response and how vigorous the response is (Liu, Tuleouva, Ramanculov, & Revzin, 2010). Interferon-gamma is commonly detected using antibody-based immunosensing techniques. Although these conventional strategies, such as ELISA have a high sensitivity for interferon-gamma, they are time consuming, require multiple steps and involve enzymes and antibodies that can be difficult to produce (Sipova, et al., 2011). It is therefore very essential to develop a sensitive, selective and simple method for detecting interferon-gamma (Yan , Wang, He, Wang, Liu, & Du, 2013). Electrochemical biosensors has emerged as an alternative for detection of tuberculosis because they can be designed to detect developing tuberculosis biomarkers, and the mechanism of detection relies on changes in electrical signals at a surface-functionalised electrode by chemical reactions (Srivastava, van Rijn, & Jongsma, Biosensor-based detection of tuberculosis, 2016). Quantum dot based biosensors have generated interest because of their many properties that has great potential in biomedical applications. Quantum dot are semiconductor materials that's size are in the nanometer range and have unique optical and electrical properties due to the quantum confinement effect. There properties include extremely bright photoluminescence, broad absorption, sharp emission spectre, good photostability and chemical stability (Liu, et al., 2010); they also have a relatively large surface area which can be used for biofunctionalization (Wang,

Hu, Lin, Roy, & Yong, 2013). These properties of quantum dots are highly advantageous when developing biosensors.

This study will focuses on the novel synthesis of indium telluri-selenide (In_3TeSe_2) alloy quantum dot and the capping of the quantum dot with L-cysteine to produce a quantum dot (QD) based aptasensor for the detection of interferon-gamma (IFN-γ) TB biomarker. This interferon-gamma aptasensor is novel as no other work has used this quantum dot as a platform for their aptasensor.

1.2. Problem Statement

The study involves the development of a fast, simple, cost effective and sensitive L-cysteine capped In_3TeSe_2 quantum dot based aptasensor for the detection of interferon-gamma TB biomarker. The detection of tuberculosis is a very important area of study because tuberculosis is one of the major diseases in the world and considering the fact that the majority of the people diagnosed with tuberculosis come from developing countries where there are no access to specialized laboratories, it is important that an alternative easy to use diagnostic approach be developed. Thus this biosensor will offer a fast, sensitive, environmentally friendly and an easy to use method for the detection of interferon-gamma TB biomarker.

1.3. Objectives

- To synthesise In_3TeSe_2 quantum dot capped with L-cysteine.
- Spectroscopic characterization of L-cysteine- In_3TeSe_2 QD by Ultraviolet-Visible (UV-Vis) absorption and Fluorescence (FL) spectroscopy and Fourier Transform Infra-red (FTIR) spectroscopy.

- Microscopic characterization of L-cysteine-In_3TeSe_2 QD by High Resolution Transmission Electron Microscopy (HRTEM) and High Resolution Scanning Electron Microscopy.
- Electrochemical characterization of L-cysteine- In_3TeSe_2 QD modified gold electrode using cyclic voltammetry, square wave voltammetry and electrochemical impedance spectroscopy.
- To develop, characterise and optimise L-cysteine-capped indium telluriselenide (In_3TeSe_2 QD)-based electrochemical DNA aptasensor for interferon gamma.
- To determine the response parameters of iFN-γ by cyclic voltammetry, square wave voltammetry and electrochemical impedance spectroscopy.

Chapter 2: Determination of Interferon-gamma, a TB biomarker.

Literature Review

2.1. Background on Interferon-gamma

Interferon-gamma is a significant inflammatory cytokine that is secreted by immune cells in response to numerous pathogens (Tuleuova, Jones, Yan, Ramanculov, Yokobayashi, & Revzin, 2010). It is a small homodimeric protein that is produced by T-cells and natural killer cells, it provides diagnostic information on several infectious diseases, therefore sensitive and accurate quantification of interferon-gamma is of great interest in diagnostics and medical research (Winterflood, Ruckstuhl, & Seeger, 2013). The traditional method of quantification of interferon-gamma over the years has been the enzyme-linked immunosorbent assay (ELISA).

2.2. Current Interferon-gamma diagnosis techniques

2.2.1. Traditional enzyme-linked immunosorbent assay (ELISA)

The ELISA test is the most common type of immunoassay used. It is used to detect proteins, antibodies and hormones and it is named ELISA due to the fact that it uses an enzyme system and immunosorbent. It is a very sensitive laboratory technique that uses microliter quantity of sample (Acharya, 2012).

ELISA is an assay technique that is performed in a 96-well microtiter plates. Different serums are incubated in each well; a positive and negative control serum is used and is among the 96 well samples being tested. Antibodies or antigens present in the serum are captured by an equivalent antibody or antigen which is coated on the solid surface. After a while the serum and unbound antibody or antigens is removed by washing the plate. For the detection of the bound antibodies and antigens, a secondary antibody conjugated to an enzyme is added to each well. After the incubation period unbound secondary antibodies

are washed off. The enzyme reacts with the substrate after its added to produce a colour end point. The colour is a measurable function of antigens or antibodies that are present in the sample (Pokhrel, 2015).

Although ELISA is a powerful technique for biomedical research and as a diagnostic tool; it detects all kinds of biological molecules at very low concentrations and quantities, it has its limitations too. The limitations include; false-positive results due to nonspecific binding of the antibody or antigen to the plate and also due to the color strength that inaccurately reflect the amount of primary antibodies present after waiting for a much extended time (Gan & Patel, 2013).

2.2.2. Interferon-gamma release assay (IGRA)

Interferon-gamma release assay is an immunological assay that is based on the principle that T-cells of individuals that is sensitised with tuberculosis antigens produce interferon-gamma when they are re-encounted with mycobacterial antigens. The amount of interferon-gamma released from CD4 and CD8 lymphocytes after stimulation with M.tuberculosis specific antigens is detected and quantified in this assay (Subramaniam, 2009). Interferon-gamma assays use to use PPD (purified protein derivative) as a stimulating antigen, however newer assays use early secretory antigenic target 6 (ESAT6) because it is specific to M.tuberculosis and culture filtrate protein 10 (CFP10). These two proteins are located within the region of difference 1 (RD1) of the M.tuberculosis genome and they are encoded by genes, thus they are considerably more specific to M.tuberculosis than PPD due to the fact that they are not shared with any bacillus calmette-guerin (BCG) substrains or most non-TB Mycobacterial species (Pai, Riley, & Colford Jr, Interferon-gamma assays in the immunodiagnosis of tuberculosis: a systematic review, 2004).

There are two interferon-gamma release assays that are commercially available in many countries: the QuantiFERON-TB Gold In-Tube (QFT) assay and the T-SPOT-TB assay, both of which have been approved by the FDA. The QFT assay is an ELISA-based whole-blood test that uses RD1 antigens (ESAT6 and CFP10) peptides as well as peptides from an additional antigen in an in-tube format. The results are expressed as IFN-γ per millimetre. The T-SPOT-TB assay is an enzyme-linked immunosorbent spot (ELISPOT) assay that uses peripheral blood mononuclear cells (PBMCs) that are incubated with ESAT6 and CFP10 peptides. The results are expressed as the number of interferon-γ producing T-cells (spot-forming cells) (Pai, et al., 2014).

Interferon-gamma assays are a useful diagnostic tool in biomedical research however it does come with its limitations and disadvantages. The disadvantages being; it does not differentiate between latent tuberculosis and active tuberculosis in patients, the specimen has to be analysed within 12 hours of collection or else the accuracy will drop, the cost is high compared to tuberculosis skin test and a large amount of blood is needed which is not acceptable for children (Subramaniam, 2009).

2.3. Biosensors in Interferon-gamma detection

2.3.1. Electrochemical biosensors

Recently over the years, electrochemical biosensors have been the centre of basic as well as applied research (Pohanka & Skladal, 2008). Electrochemical biosensors are sensing devices that couples a biological recognition element to an electrode transducer, the transducer then converts the biological recognition event into an electrical signal (Wang J. , 2006). A typical biosensor comprises of; a bioreceptor that binds to the analyte, an interface architecture where the biological reaction takes place which then gives off a signal, a transducer; the transducer signal is converted to an electric signal and amplified by a

detector circuit, computer software to convert the processes into a meaningful physical parameter and an interface to the human operator. Biosensors can be applied to a variety of samples which include body fluids, cell cultures and much more (Grieshaber D. , MacKenzie, Voras, & Reimhult, 2008). The schematic of the parts present in a biosensor is shown in **Figure 1**.

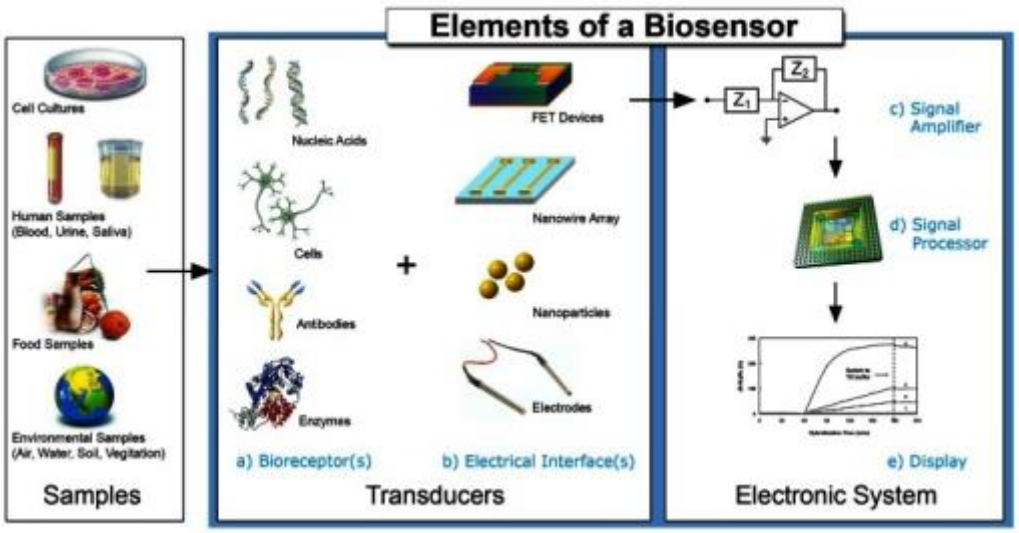

Figure 1: Schematic representation of the elements of a typical biosensor (Grieshaber D. , MacKenzie, Voros, & Reimhult, 2008).

Based on the measuring electrical parameters, electrochemical biosensors can be categorized as; conductimeric, amperometric and potentiometric. Conductimetric biosensors measure electrical conductance/resistance of the solution. The overall conductivity/resistivity of a solution changes when the electrochemical reaction produces ions or electrons. This change is then measured and calibrated to a proper scale. Amperometric biosensors are the most commonly used electrochemical detection method. This biosensor has high sensitivity and can detect electroactive species present in biological samples. It produces a current proportional to the concentration of the substance. Potentiometric biosensors measure the oxidation/reduction potential of an electrochemical reaction. The working principle of this biosensor relies on the fact that when a voltage is

applied to an electrode in a solution the current flows due to the electrochemical reactions and the voltage at which the reaction occurs indicates a particular reaction and particular species (Darsanaki, Azizzadeh, Nourbakhsh, Raeisi, & Aliabadi, 2013).

The electrochemical sensing requires a reference, working and counter electrode. The reference electrode which is usually Ag/AgCl is kept at a distance from the working electrode so that it can uphold a known and stable potential. The working electrode is the transduction element where the reaction occurs, and the counter electrode creates a connection to the electrolytic solution so that the current can be applied to the working electrode. The electrodes should be conductive and chemically stable (Grieshaber D. , MacKenzie, Voras, & Reimhult, 2008).

2.3.1.1. Aptamer based electrochemical biosensors

Aptamers have become essential molecular tools for diagnostics and therapeutics, but in particular aptamer based biosensors is much more advantageous than biosensors that use natural receptors like antibodies and enzymes because of their high specificity and affinity for any target (Song , Wang, Li, Zhao, & Fan, 2008). The intrinsic properties of aptamers include high flexibility of structure and convenience in the design of their structure which enables researchers to develop various novel aptasensors. Once aptamers bind to their target they fold into well-defined 3D structure and their conformation is very flexible depending on the target molecules (Kim, Raston, & Gu, 2016). Aptamer based electrochemical biosensors offers great sensitivity, signal stability and ease of calibration (Liu, Tuleouva, Ramanculov, & Revzin, 2010).

Liu et al. (2010) developed an electrochemical DNA aptasensor to detect interferon-gamma. They had a DNA-hairpin that contained thiolated interferon-gamma aptamer. The aptamer

was conjugated with a redox label; methylene blue (MB) and was immobilized on a gold electrode by self-assembly. The aptamer assembly and IFN-γ binding was analysed using surface plasmon resonance experiments and the electrochemical aptasensors response was analysed using square wave voltammetry. What they found from the surface plasmon resonance experiments was that the binding of the cytokine to the aptamer was not hindered by the attachment of methylene blue. They also found that the binding of IFN-γ caused the hairpin to open, thus moving the redox tag away from the electrode surface and ultimately decreasing the current at the electrode. Their aptasensors had a linear range that extends to 10 nM and LOD of 0.06 nM. Their aptasensor had a high specificity to interferon-gamma even in the presence of other proteins; it could also be regenerated by treatment with urea buffer and reused numerous times. Their aptamer-based biosensor was sensitive and specific to interferon-gamma, even in the presence of high concentrations of serum proteins (Liu, Tuleouva, Ramanculov, & Revzin, 2010).

Farid et al. (2015) produced a DNA aptamer-based electrochemical biosensor to detect interferon-gamma, however there interferon-gamma binding aptamer was attached to a graphene platform. The graphene platform comprised of a graphene monolayer-based field effective transistors (FET) like structure that was integrated on a polydimethylsiloxane (PDMS) substrate. The binding of the aptamer to graphene was verified using atomic force microscopy (AFM), to make sure that the aptamers were properly immobilized on the graphene surface. Their findings were that; when they added their target molecule, interferon-gamma there was a change in charge distribution in the electrolyte that resulted in an increase in electron transfer efficiency and also causing a current change across the graphene. The change in current was detected and it was found to be dependent on the

concentrations of interferon-gamma. The limit of detection of the biosensor was found to be 83 pM making their biosensor very sensitive to interferon-gamma (Farid, et al., 2015).

Both aptamer-based electrochemical biosensors developed from these two groups were specific to interferon-gamma, even in the presence of other proteins and they produced biosensors with good sensitivity which will be helpful in my research study.

2.3.2. Electrochemical immunosensors

Electrochemical immunosensors have gained a considerable amount of interest due to the fact that they are specific to antigen-antibody recognition and have high sensitivity of electrochemical methods, for this reason there have been significant progress in the early diagnosis and clinical analysis of diseases. Electrochemical immunosensors have provided the detection of trace amounts of analytical targets of biological significance that ranges from macromolecules, small molecules, viruses or cells (Wen, Yan, Zhu, Du, & Lin, 2017).

Immunosensors are antibody-antigen based affinity biosensors, where the detection of the antigen as target analyte is a result of the specific binding of the antigen to an antibody on the electrode surface. In electrochemical immunosensors the antibody acts as the bioreceptor and the antigen as a target analyte and the transducer can quantify the antigen concentration by using amperometric, potentiometric, conductometric or impedimetric signals, a schematic of the electrochemical immunosensor is shown in **Figure 2**. Electrochemical immunosensors are easy to use, simple, portable and cost effective. The method of immobilization of antibodies is crucial to the design of the immunosensor, these methods include; physical and chemical adsorption (Bahadir & Sezginturk, Applications of electrochemical immunosensors for early clinical diagnosis, 2015). Physical adsorption can be accomplished by attaching molecules directly to the surface or by forming a complex

with other particles. The adsorption of antibodies on the surface is achieved via van der Waals force, hydrophobic interaction, hydrogen bonding and electrostatic interactions (Gopinath, Tang, Citartan, Chen, & Lakshmipriya, 2014).

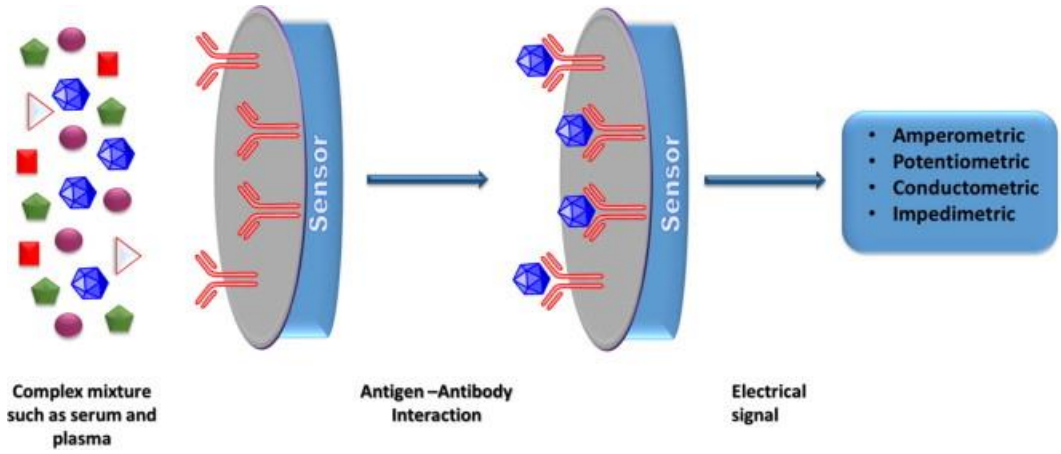

Figure 2: Schematic representation of an electrochemical immunosensor (Bahadir & Sezginturk, 2015).

2.3.2.1. Quantum dot based immunosensor

In immunosensors, nanoparticles can serve as; i) modifiers of the electrode surface by acting as electrochemical catalysts to enhance electron transfer kinetics of a reaction, ii) as carriers of enzyme labels and as electrochemical labels (Kokkinos, Economou, & Prodromidis, 2016). That is why many kinds of nanomaterials, including metal nanoparticles, quantum dot, carbon nanotubes and magnetic nanobeads have widely been used in electrochemical immunosensors because these labels provide signal amplification compared to the traditional enzyme labels and redox probe labels. As can be seen by *Yang.(2015) who* developed an electrochemical impedance immunosensor that is based on cylinder-shaped TiO_2 nanorods to detect bovine interferon-gamma. The bovine interferon-gamma antibody was immobilized on the TiO_2 modified electrode which improved the sensitivity of the immunosensor because the TiO_2 provided a hydrophilic, favourable and high capacity platform for the loading of the proteins. Their immunosensor exhibited high sensitivity for

the determination of bovine interferon-gamma and displayed a limit of detection of 0.1 pg/mL (Yang, et al., 2015).

Quantum dot displays exceptional fluorescence, optical properties, good photo stability and a high emission intensity, all of these which is advantageous in biological applications (Rakesh Dhar, 2014). These properties of quantum dot are advantageous in the development of new and improved sensors. Developing multiple probes that link recognition molecules like nucleic acids, peptides or small-molecule ligands is encouraged by the surface chemistry of luminescent quantum dot (Baghar, 2016). Quantum dot have been used in immunosensors because of the unique properties that they possess. Their intrinsic redox properties and sensitive electrochemical stripping analysis of the metal components of the semiconductor nanoparticles (CdS, PbS and ZnS) cause the labels in the electrochemical biosensors to be very sensitive (Liu & Lin, 2007). *Huang et al.* developed an immunosensor using CdS quantum dot coupled to magnetic beads as electrochemical labels for the detection of interferon-gamma. Their sandwich type immunosensor showed a linear relationship with the logarithm of the interferon-gamma concentrations and the detection limit they achieved was 0.34 pg mL^{-1} indicating that the sensitivity of their immunosensor was significantly high (Huang, et al., 2015).

2.3.3. Optical biosensors

Optical biosensors is one of the most common class of biosensors reported, they offer many advantages over conventional analytical techniques because of their direct, real-time and label-free detection of biological and chemical substances. Optical biosensors advantageous include; high specificity, small size, high sensitivity and cost effectiveness. Optical detection is achieved by exploiting the interaction of the optical field with a biorecognition element (Damborsky, Svital, & Katrilik, 2016).

Optical biosensors are an analytical device that has a biological sensing element integrated to an optical transducer system (Dey & Goswami, 2011). An optical biosensor comprises of: a light source, optical transmission medium, immobilized biological recognition element (enzymes or antibodies) and an optical detection system (Patel, Mishra, & Mandloi, 2010). The purpose of the optical biosensor is to generate an electronic signal that is proportional in magnitude to the concentration of a specific analyte or groups of analytes to which the biosensing element binds. Optical biosensors can be classified according to their biorecognition system (Dey & Goswami, 2011).

Optical biosensors are a powerful analytical detection technique and analysis tool that has a variety of applications in biomedical research, healthcare, pharmaceuticals and environmental monitoring. They are immune to electromagnetic interference, are capable of performing remote sensing and it can provide multiple detection within a single device. There are two detection methods that's applied in optical biosensing and they include; fluorescent-based detection and label-free detection. In fluorescent-based detection the target molecules or biorecognition molecules are labelled with fluorescent tags; the presence of the target molecules and the interaction strength between the target and biorecognition molecules is indicated by the intensity of the fluorescence. In label-free detection the target molecules are detected in their natural forms since they are not labelled or altered (Fan, White , Shopova, Zhu, Suter, & Sun, 2008).

2.3.3.1. Surface plasmon resonance (SPR) biosensors

R. Wood. (1902) was the first documented person to observe surface plasmons back in the early 1900's; he unexplained the narrow dark bands in the diffracted spectrum of metallic gratings that were illuminated with polychromatic light (Wood, 1902). The application of surface plasmon resonance for biosensing was later demonstrated in 1983, but since then

the surface plasmon resonance (SPR) sensor technology for the detection of chemical and biological substances has been extensively studied and has generated quite an interest from the science community. Surface plasmon resonance biosensors are employed in many important applications such as; biology, food safety and medical diagnostics (Wijaya, et al., 2011).

In SPR biosensing, the adsorption of a targeted analyte by a surface bioreceptor is measured by tracking the change in the conditions of the resonance coupling of incident light to the propagating surface plasmon wave (SPW). The surface plasmon wave is dictated by the electromagnetic properties of a metal, usually gold or silver, and a dielectric (sample medium) interface. The resonance coupling which appears as a dip in the reflectivity of the light spectrum is tracked by measuring the wavelength, the incident angle or the intensity of the reflected light. A high-index prism or a periodic grating surface is required for the coupling of the light to the surface plasmon wave (Hoa, Kirk, & Tabrizian, 2007). The SPR instrumentation contains a convergent monochromatic beam that's directed onto the prism coupler, over which the sample containing the metal layer modified with receptor molecule is passed (Srivastava, van Rijn, & Jongsma, Biosensor-based detection of tuberculosis, 2016). The SPR representation is displayed in **Figure 3**.

There are four different methods used for the excitation of surface plasmon resonance and they include; prism coupling, waveguide coupling, fibre optic coupling and grating coupling. In the prism coupling configuration, an evanescent field is generated that penetrates into the metal layer due to the incident being totally reflected at the prism-metal interface. The photon is coupled into the surface plasmon wave. In the waveguide coupling, the light propagates through total internal reflection and generates an evanescent field at the

waveguide-metal interface which excites the surface plasmon wave in the same way as in the prism configuration. In the fibre optic coupling the surface plasmon wave is excited in an easy and flexible way. A small portion of the fibre is removed and coated with a layer of metal film. In the grating coupling the incident light directly illuminates the metal surface and requires the sample fluid and microfluidics to be optically transparent (Fan, White , Shopova, Zhu, Suter, & Sun, 2008).

Sipova et al. (2012) developed a SPR biosensor that used engineering proteins to directly detect interferon-gamma in diluted blood plasma. The proteins were derived from albumin binding domain (ABD) of protein G and were immobilized directly onto the SPR biosensor for the direct detection of human interferon-gamma. Their biosensor detected human IFN-γ in both buffer and diluted human plasma and they received a LOD of 0.2nM *(Sipova, et al., 2012).* The same group developed another SPR biosensor based on engineered proteins to detect human interferon-gamma in buffer and also in diluted human plasma but in this instance they selected the proteins with ribosome display to provide high affinity towards human interferon-gamma. Their biosensor displayed a limit of detection of 1nM in buffer and 10nM in diluted plasma *(Sipova, et al., 2011).*

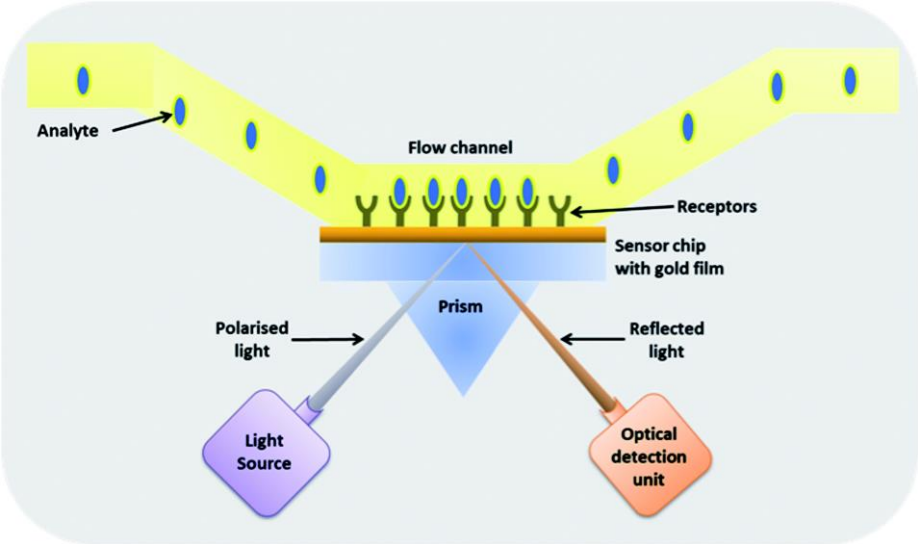

Figure 3: Schematic representation of a surface plasmon resonance based biosensor (Srivastava, van Rijn, & Jongsma, 2016).

2.3.3.1.1. Amplified surface plasmon resonance immunosensor

Immunosensors that use antibodies as the biological recognition element is the most common biosensing method used to detect protein. Surface plasmon resonance technique can be combined with immunosensors to reach high sensitivity and real-time detection of proteins (Xia, Zun-zhong, Jian, & Yi-bin, 2010).

Surface plasmon resonance immunosensors have been receiving interest for a variety of reasons that include selectivity, reliability in analysis with additional emphasis on portability, miniaturization and on-site analysis. Surface plasmon resonance based immunosensors has a high specific detection for small molecules that have low detection limits for a wide variety of analytes in complex matrices. In a SPR immunosensor when the antibody that is immobilized on the surface binds to the analyte, the change in the interfacial refractive index is detected as a shift in the resonance angle. These changes are then monitored over time and eventually converted into a sensorgram, and from the sensorgram the kinetics and affinity constants of the interaction can be determined. The resonance angle shift provides information on: the affinity of the analyte for the antibody, the amount of bound analyte

and the association and dissociation kinetics between the antibody and analyte (Shankaran, Gobi, & Miura, 2007).

Some surface plasmon resonance biosensors use an amplifying agent like aptamers for example to amplify the signal and to enhance the surface plasmon resonance response (Chang, et al., 2012). That is what Chang and colleagues did; they developed an amplified surface plasmon resonance immunosensor to detect interferon-gamma in pure buffer and plasma dilutions the biosensor was based on a streptavidin-incorporated aptamer. They used a bifunctional, combined aptamer system. Their target molecules induced the refolding of the aptamer probe to a binding conformation of the streptavidin (SA) aptamer in the presence of interferon-gamma, which lead to surface plasmon resonance responses that were further improved upon by the binding of the SA molecules to the aptamer probes. They achieved a LOD of 33 pM and their sensor had a high sensitivity, was simple and reusable (Chang, et al., 2012).

Chapter 3

Experimental

3.1. Chemicals

The chemicals used in this study are analytical grade sodium hydroxide (NaOH), granular 99% sodium borohydride ($NaBH_4$), anhydrous indium(III) chloride powder, 99% metal basis tellurium (Te) powder, 99% selenium (Se) powder, 98.5% L-cysteine powder, 98% 1-ethyl-3-(3-dimethylaminopropyl) carbodiimide hydrochloride (EDC), 98% N-hydroxysuccinimide (NHS), 2-propanol, 99.5% disodium hydrogen phosphate (Na_2HPO_4), 99% sodium dihydrogen phosphate (NaH_2PO_4), 99% 6-mercapto-1-hexanol (MCH) and Streptavidin ($\geq$ 13 units/mg protein) were all purchased from Sigma Aldrich (South Africa). The biotinylated aptamers (MW = 28 062.2 g/mol) with sequence 5'-/Biosg/GCC TGT TGT GAG CCT CCT AAC CTT TAT GAC GGT CTA TAC GCT CTG GTG CAA TTG and the interferon-gamma (MW = 17 145.6 g/mol) were received from the Lung Infectious Unit of the University of Cape Town Lung Institute.

3.2. Materials and Instrumentation

All electrochemical experiments were carried out using PalmSens BV compact electrochemical interfaces, GA Houten (Netherlands). Both cyclic, square wave voltammograms and electrochemical impedance spectrums were recorded with a computer interfaced to the PalmSens electrochemical workstation.

A three electrode set-up was used, the electrodes included:

- Ag/AgCl (3M KCl) reference electrode from BAS
- Platinum wire counter electrode from Sigma Aldrich
- Gold working electrode (A = 0.0201 cm^2) from BAS

Analytical grade argon gas that was used to degas the cell solution was purchased from Afrox Company, South Africa. The Alumina polishing pads and powders (1 µM, 0.3µM and 0.05µM) that were used to clean the electrode surface were purchased from Buehler, Illinois, USA.

CV, SWV and EIS measurements were recorded with PalmSens electrochemical interface (Netherlands). UV-Vis absorption measurements were made on a Nicolet Evolution 100 UV-Vis spectrometer (Thermo Electron, UK) using a quartz cuvette. FL spectra were recorded using Horiba NanoLog™ 3-22- TRIAX (USA). FT-IR spectra were recorded on PerkinElmer spectrum 100, FT-IR spectrometer. Microwave irradiation was done using Multiwave PRO, Anton Paar (Graz-Austria). HR-TEM analyses were done using a Tecnai G2 F20X-Twin MAT 200 kV Field Emission Transmission Electron Microscope from FEI (Eindhoven, Netherlands). SaxSpace Anton Paar (Austria).

3.3. Method

3.3.1. Synthesis of L-cysteine capped In_3TeSe_2 QD

The L-cysteine capped In_3TeSe_2 QD is prepared according to a method described by (Yang, Yang, & Cao, 2013), (Fang, Liu, Xu, Yin, & Zhong, 2008) with modifications.

3.3.2. Preparation of Sodium hydrogen telluride (NaHTe) and Sodium hydrogen selenide (NaHSe)

The Te source is prepared by mixing Te powder and $NaBH_4$ in a 1:3 (mol/mol) ratio in a three-necked round bottom flask. The air in the system is pumped off and replaced with N_2 gas before and after loading of the powders. Distilled water is added to the flask through a syringe and the reaction mixture is stirred at room temperature under N_2 gas to get a deep purple solution. Similarly Se source is prepared by combining Se powder and $NaBH_4$ in a 1:3 (mol/mol) ratio in a three-necked round bottom flask and the air pumped off using N_2 gas

before and after the loading of the powders. Distilled water is added through a syringe and the reaction mixture is magnetically stirred at room temperature under N_2 flow until an orange clear solution is observed.

3.3.3. Microwave Synthesis of L-cysteine capped In_3TeSe_2 QD

Typically $InCl_3$ and L-cysteine is dissolved in 20 ml of distilled water, an ultrasonic cleaner is used to accelerate the dissolution of L-cysteine followed by the pH adjustment of the solution to 11.5 through drop-wise addition of 2M NaOH solution. The resulting solution is degassed with N_2 and mixed for at least 60 min at room temperature under magnetic stirring.

The freshly prepared NaHTe and NaHSe solutions are injected simultaneously into the L-cysteine capped $InCl_3$ solution using two syringes with violent stirring at anaerobic condition. The mixture is stirred for a few minutes before being transferred into Teflon vessels and undergoes microwave irradiation for 30 min at 100 ˚C. After irradiation, the L-cysteine capped In_3TeSe_2 QD samples are taken out when the temperature of the system was 55 ˚C. The as prepared L-cysteine capped In_3TeSe_2 alloyed QD is precipitated and washed with 2-propanol and dried overnight at room temperature in a vacuum.

3.4. Sample Preparation

3.4.1. Preparation of electrolyte buffer solution

A 0.1 M phosphate buffer solution (PBS), pH 7.4 was prepared from Na_2HPO_4 and NaH_2PO_4 and was used as the electrolyte solution throughout the course of this study. The phosphate buffer electrolyte solution was kept refrigerated at -4 ˚C when not in use.

3.4.2. Preparation of stock and working solutions

A 1 μM of biotinylated aptamer solution were prepared by adding 992.3 μL of 0.1 M PBS buffer solution to the biotinylated aptamer stock solution of 1.3 $x10^{-4}$ M. A 17 μM

streptavidin stock solution was prepared; 60 µL of the stock streptavidin was added to 940 µL of PBS buffer solution to make a 1 µM working solution. A 100 ng/mL of interferon-gamma stock solution was prepared followed by the preparation of a 1 ng/ml of Interferon-gamma working solution by adding 900 µL of PBS buffer solution to the interferon-gamma solution. The working solutions were kept in the fridge at -4 ˚C when not in use.

3.5. Fabrication of L-cysteine-In_3TeSe_2 QD Aptasensor and electrochemical detection

The gold electrode is cleaned by polishing with 1, 0.3 and 0.05 µM alumina slurries on polishing pads, rinsing with ethanol after each polish. This is followed by ultrasonification in deionized water for 5 min. The freshly polished gold electrode is then electrochemically cleaned in 0.5 M sulphuric acid by potential scanning between -400 and 1400 mV until reproducible cyclic voltammagrams are obtained. The gold electrode is then immersed in L-cysteine-In_3TeSe_2 QD solution for 12 h at room temperature to obtain an AuE/L-cysteine-In_3TeSe_2. The modified gold electrode is rinsed with ultra-pure water to get rid of any unbound quantum dots. The AuE/L-cysteine-In_3TeSe_2 is then immersed in a 1:1 EDC and NHS solution to activate the QD. The surface activated electrode is rinsed with ultra-pure water again. 20 µL of the streptavidin solution is drop-coated on the modified electrode and incubated for 2 h. After that 20 µL of the biotinylated aptamer solution is drop-coated onto the electrode as well and left overnight so that the streptavidin can bind to the biotin molecules on the aptamer. Following that, 20 µL of 6-Mercapto-1-hexanol solution was drop-coated onto the modified electrode and incubated for an hour after which it was rinsed with ultra-pure water to give AuE/L-cysteine-In_3TeSe_2/Aptamer biosensor. The QD aptasensor was then complete and ready for electrochemical detection of Interferon-gamma. Detection was carried out by immersing the QD aptasensor in a stirred solution of

0.1 M PBS buffer solution containing different concentrations (0.25-1.5 pg/mL) of interferon-gamma for 5 min and electrochemically detected by carrying out CV, SWV and EIS studies on the AuE/L-cysteine-In_3TeSe_2/Aptamer biosensor. A schematic representation of the fabrication of the L-cysteine-In_3TeSe_2 QD based Aptasensor is displayed in **Figure 4** below.

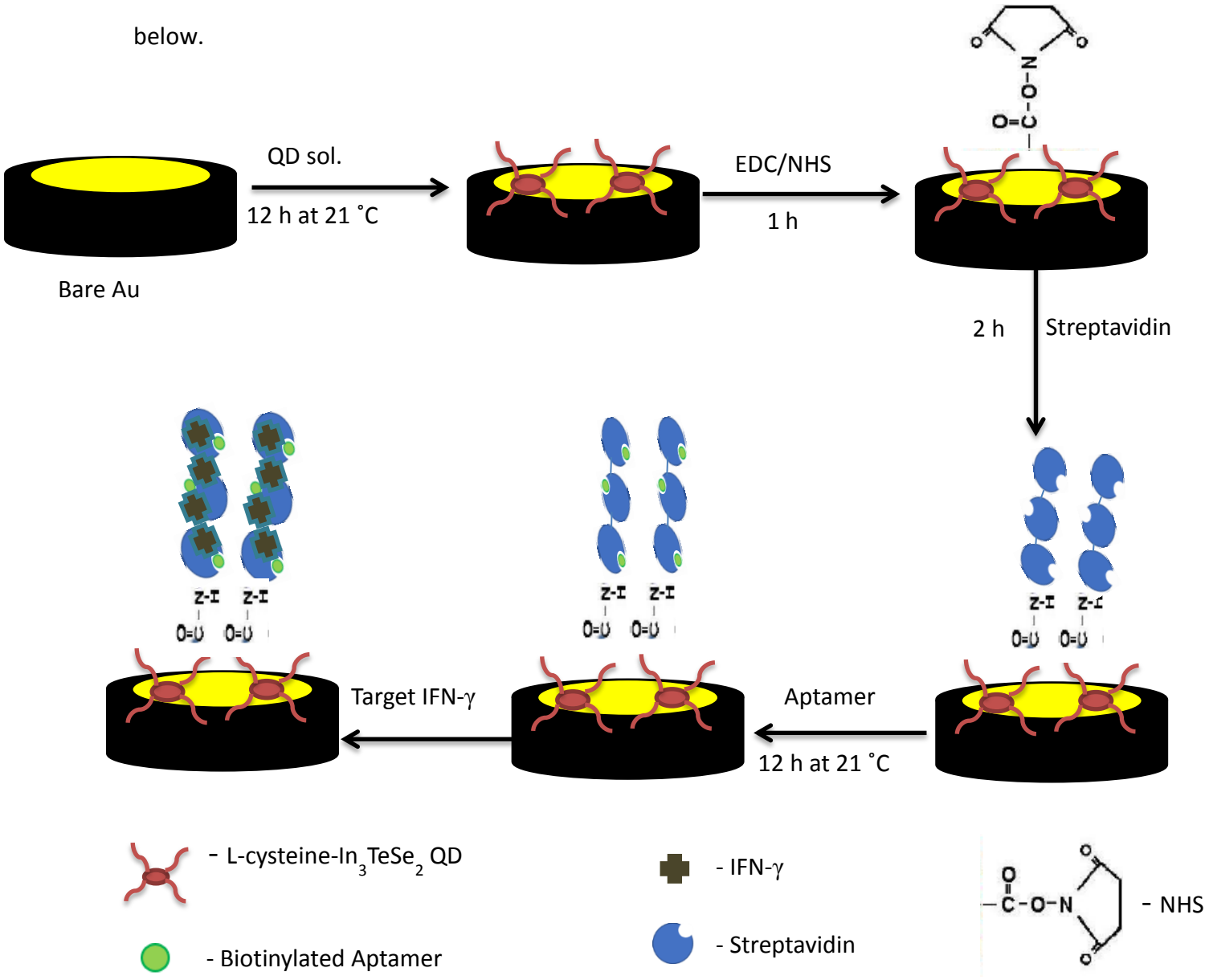

Figure 4: Schematic representation of the fabrication of L-cysteine-In_3TeSe_2 QD based aptasensor.

Characterization techniques

A variety of characterization techniques such as UV-Vis, PL, FTIR, SaxSpace and HRTEM has been used in this study to characterize the quantum dots. The quantum dot along with the application of the electrochemical QD aptasensor was studied using various electrochemical techniques such as CV, SWV and EIS. The following is a brief overview of the principles of these characterization techniques.

3.6. Spectroscopic Techniques

3.6.1. Ultraviolet-Visible Spectroscopy (UV-Vis)

UV-Vis is an analytical technique used to measure the absorbance of a material as a function of the wavelength. It also allows you to determine the concentrations of a substance and the rates of a reaction from which a mechanism can be proposed. This technique is simple, flexible, low cost, and convenient and is used in a wide range of scientific areas. It is used extensively in research and analytical laboratories for the quantitative analysis of molecules that absorb ultraviolet and visible electromagnetic radiation (Pena-Pereira, Costas-Mora, Romero, Lavilla, & Bendicho, 2011).

In this research study UV-Vis was used to study the spectroelectro properties of L-cysteine-In_3TeSe_2 QD. The QD was dissolved in water and placed in a 4 cm^3 quartz cuvettes and distilled water was used as the blank throughout. The UV-Vis absorption spectra of these QD were recorded in the region of 200-600 nm.

3.6.2. Fluorescence Spectroscopy (PL)

Fluorescence is the molecular absorption of light energy at one wavelength and the emission at another wavelength. Fluorescent compounds have two characteristic spectres; an excitation spectre (the amount of light being absorbed) and an emission spectre (amount of light being emitted).

The absorption and emission of energy are characteristics that are unique to a particular molecule during the fluorescence process. The molecules absorb light causing electrons to become excited to a higher electronic state, they remain in the excited state presuming that all the excess energy is not lost by collisions with other molecules, then the electrons return to the ground state. On the electrons return to the ground state energy is emitted.

Fluorescence is an analytical technique that is known for its extraordinary sensitivity, high specificity, simplicity and low cost compared to other analytical techniques. It is a technique that is widely accepted, powerful and is used in various applications such as environmental and industrial. It is an analytical tool that is used for both quantitative and qualitative analysis (Alexeiv & Farrens, 2014).

In this research study PL was used to investigate the fluorescent ability of L-cysteine-In_3TeSe_2 QD. The sample was placed in a 400µL quartz cuvette and the PL was recorded with double grating emission monochromator at a slid width of 5nm. The PL spectre was measured on the QD solution that was diluted with water to obtain an appropriate PL measurement, distilled water was used as the blank throughout.

3.6.3. Fourier Transform Infrared Spectroscopy (FTIR)

Fourier Transform Infrared Spectroscopy (FTIR) is an analytical technique that measures the vibrations and associated overtones of a chemical species that is present in the sample in the infrared region of the electromagnetic spectrum (von Aulock, et al., 2014). In infrared spectroscopy, IR radiation is passed through a sample. Some of this radiation is absorbed by the sample while the others are transmitted. The resulting spectrum represents the molecular absorption and transmission. Each IR absorption peak is determined by intrinsic physicochemical properties of each corresponding molecule and thus acts as a molecular

fingerprint for that specific molecule (Chen, Zou, Mastalerz, Hu, Gasaway, & Tao, 2015). No two compounds produce the same infrared spectrum; therefore this technique is useful in positive identification of every different kind of material. The only major disadvantage of this technique is related to the sample preparation; it requires that the supported wafer by thin and doubly polished, otherwise the quantitative measurements won't be as accurate (von Aulock, et al., 2014). A schematic representation of the essential features in a FTIR spectrometer is shown in **Figure 5** below.

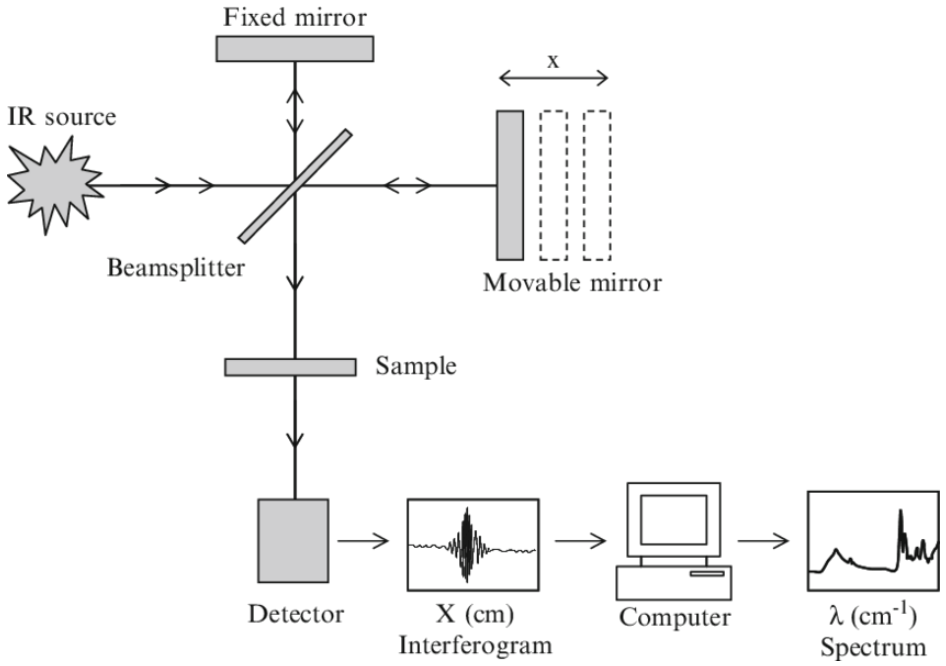

Figure 5: Schematic representation of important features in a FTIR spectrometer (Ojeda & Dittrich, 2012).

In this research study FTIR spectroscopy was used to investigate if the In_3TeSe_2 QD was capped with the surfactant L-cysteine. The FTIR analysis was done on liquid samples of L-cysteine-In_3TeSe_2 QD which were dropped through a syringe onto the crystal window of the device. The FTIR spectra were recorded from a frequency range of 4000-400 cm^{-1}.

3.7. Structural Techniques

3.7.1. Small angle X-ray Scattering (SAXS)

Small angle x-ray scattering (SAXS) is an analytical technique that determines the structure of particles in terms of average particle size or particle shape. The samples can be solid, liquid and can contain solid, liquid or gaseous domains of the same or another sample in any combination. X-rays are sent through the sample and each particle in the beam will send out its signal measuring the average structure of all particles illuminated in the bulk material. SAXS is a non-destructive and accurate analytical technique, requiring only a minimum of sample preparation. It has a broad area of application which includes; polymers, nanocomposites, metals and biological materials (Schnablegger & Singh, 2011).

In this research study SAXS was used to study the size and shape of the QD. The SAXS analysis was done on powder samples of L-cysteine-In_3TeSe_2 QD and was obtained using a 1 mm diameter quartz capillary positioned at a distance of 317 mm from the SDD camera and temperature-controlled at 20 °C. Measurements were performed with the SAXSpace system (Anton Paar, GmbH, Australia) in line-collimation mode with an accessible q range of 0.0732–1.66 nm. For each measurement, six frames were obtained at 100 s exposure time and averaged. The blank tape was measured as a reference under the same conditions as the sample. Data evaluation/analysis was performed with the GIFT software (generalized indirect Fourier transformation (GIFT) which is a versatile tool for the evaluation of small angle scattering data) in order to determine the particle size and the size distribution of the dispersions.

3.8. Microscopic Techniques

3.8.1. High Resolution Transmission Electron Microscopy (HRTEM)

In Transmission Electron Microscopy (TEM) a beam of electrons is passed through a thin specimen interacting with the sample as it passes through. When the electrons are transmitted through the sample an image is formed; the image contrast depends on the structure, thickness, composition of the specimen as well as the imaging parameters. In high resolution transmission electron microscopy imaging, the objects are required to be very thin which depends on their properties (Hettler, Dries, Zeelan, Oster, Schroder, & Gerthsen, 2016).

A modern Transmission Electron Microscope (TEM) consists of an illumination system, specimen stage, objective lens system, data recording system, magnification system and the chemical analysis system. The illumination system comprises of the electron gun which uses LaB_6 thermionic emission source or a field emission source. The illumination system also comprises the condenser lenses that are very important for forming a fine electron probe. The specimen stage carries out the structure analysis; it can be used to perform observations that are induced by annealing, electric field or mechanical stress, providing the possibility of characterizing the physical properties of nanostructures. The objective lens system determines the limit of image resolution. The magnification system contains the intermediate lenses and projection lenses that give a magnification of up to 1.5 million. The data recording system is digital and uses a charge coupled device (CCD) that allows quantification and quantitative data processing. The chemical analysis system is the energy dispersive X-Ray spectroscopy (EDS) that is used to determine the chemical composition of the specimen (Wang Z. , 2000).

In this study HRTEM was used to investigate the shape, size and structure of the QD. It was also used to determine the elemental composition of the QD. A copper grid was used as the platform for sample preparation, the L-cysteine-In_3TeSe_2 QD solution was drop coated onto the grid and allowed to dry by leaving it for 15 min under a lamp before performing HRTEM analysis.

3.8.2. High Resolution Scanning Electron Microscopy (HRSEM)

The scanning electron microscope is very versatile and is the most widely used electron beam instrument in the world in materials and life science (Bagner, Jouneau, Thollet, Basset, & Gauthier, 2007). The micrograph that is generated from this technique is easily interpreted, it produces a variety of types of information and the images and analytical information can be readily combined. Using scanning electron microscopy for material characterization you can obtain not only the images but quantitative information in two or three dimensions about the microstructure, chemistry and crystallography of the material in interest.

The principles of the scanning electron microscopy have been described by Smith and Oatley (1955). Their microscope had two electrostatic lenses to focus an electron probe onto the surface of a bulk specimen. The probe is scanned across the surface of the specimen and the electrons that emerge is collected and amplified in an electron multiplier. The signal derived is used to control the brightness of the display cathode-ray tube whose spot is scanned in synchronism with the electrode probe on the specimen. The magnification of the instrument is given by the ratio of the scanned amplitude on the display tube to that on the specimen and is varied by attenuating the current in the coils that is used to scan the electron probe. The resolution is dependent on the probe diameter. Focusing is carried out by viewing the image on the screen of the display cathode-ray tube

directly, using a scan frequency of 1 frame per second. For the photographic recording a single frame scan that lasts a few minutes was generally used. This practice was used in later scanning microscopes (Pease & Nixon, 1965).

HRSEM was used to study the surface morphology of the L-cysteine-In_3TeSe_2 QD, it was also used to determine the elemental composition of the QD. Carbon tape mounted onto aluminium stubs was the platform for sample preparation; the powdered QD was spread over the stubs before performing HRSEM analysis.

3.9. Electrochemical Techniques

3.9.1. Cyclic Voltammetry (CV)

Cyclic Voltammetry has become a very popular electrochemical technique for providing information about electrode reaction kinetics (Nicholson, 1965). Cyclic voltammetry is a very versatile technique, allowing one to probe the mechanics of redox and transport properties of a system in solution. This is accomplished using a three electrode system where the potential relative to the reference electrode is scanned at a working electrode while the resulting current flow through the counter electrode is monitored in an inactive solution.

In CV the potential of the working electrode is changed linearly with time starting from a potential where no electrode reaction occurs, moving to a potential where oxidation and reduction takes place. After the reactions take place the linear sweep is reversed and the electrode reactions of the intermediates and products that are formed during the forward scan can be detected. The time scale of the voltammogram is controlled by the scan rate and the total potential. A supporting electrolyte is used during the experiment to prevent the migration of charged reactants and products (Evans, O'Connell, Petersen, & Kelly, 1983).

The main principle of this technique is to investigate the oxidation and reduction processes of the electrode under various conditions such as the presence of intermediates in oxidation-reduction reactions and the reversibility of the reaction. The advantages of the technique include the low cost of the instrumentation however this technique cannot determine the mechanism of two or more closely spaced charge transfer reactions. There is also a concentration limit of 10 μM that needs to be adhered to in order to get information that is reliable except for when the analyte is confined to the electrode surface (Helfrick & Bottomly, 2009).

The cyclic voltammogram as shown in **Figure 6** is characterized by several important parameters such as the cathodic ($E_{p,c}$) and anodic ($E_{p,a}$) peak potentials and the cathodic ($I_{p,c}$) and anodic ($I_{p,a}$) peak currents that can be exploited to further understand the reaction kinetics occurring at the working electrode.

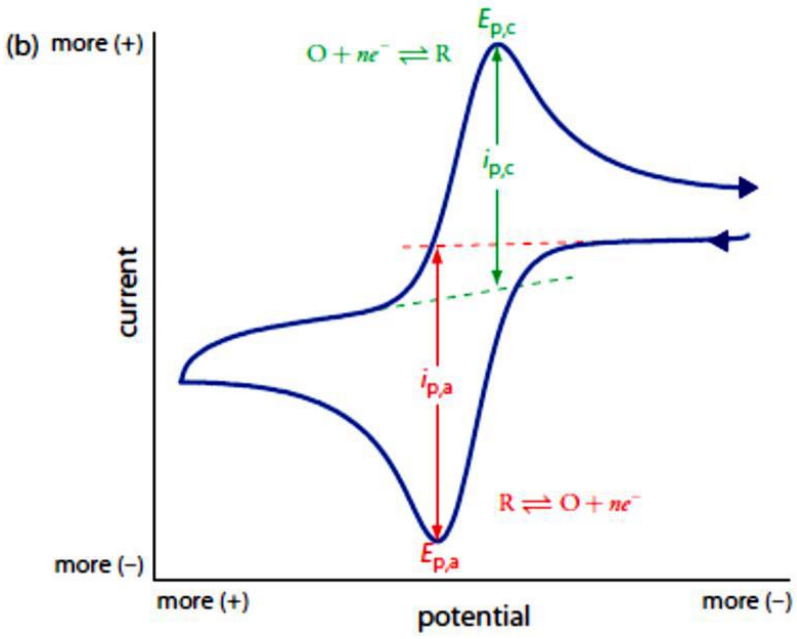

Figure 6: A typical cyclic voltammogram for a reversible redox system (Harvey, 2017).

In this study the electrochemical characterization of the L-cysteine-In_3TeSe_2 QD was carried out in 5 mL of 0.1 M PBS solutions, pH 7.4 electrolyte solution. The AuE/L-cysteine-In_3TeSe_2 QD was scanned from -1.0 V to 1.5 V at different scan rates (0.01-0.25 V/s). The AuE/L-cysteine-In_3TeSe_2 QD and AuE/L-cysteine-In_3TeSe_2 QD/Aptamer was scanned from -1.0 V to 1.5 V in 5 mL PBS solution, pH 7.4 at a fixed scan rate of 0.04 V/s for comparison reasons. Reader should bear in mind that the materials (QD and QD Aptasensor) are surface confined to the AuE. The application of the AuE/L-cysteine-In_3TeSe_2 QD/Aptamer towards different concentrations of IFN-γ was carried out in 8 mL of 0.1 M PBS, pH 7.4 over a potential range of -1.0 to 1.5 V at 0.04 V/s. The QD Aptasensor/AuE was allowed to stay for 5 min in the

electrolyte solution that contained different concentrations of IFN-γ. All CV measurements were done at room temperature. The electrolyte solution was degassed with nitrogen for at least 15 min before an electrochemical experiment.

3.9.2. Square Wave Voltammetry (SWV)

Square Wave Voltammetry (SWV) is a pulse voltammetry technique that has a lot of advantages that includes high sensitivity, great speed and a low detection limit (Suroviec, 2013). Compared to CV it has a broader dynamic range and lower detection limit because of its discrimination of capacitance current. It is also the most regularly used pulse voltammetry technique because of its short scan rate time. Due to the high sensitivity and swiftness of SWV makes this a technique that is very useful for the analysis of drugs and biological samples (Dogan-Topal, Ozkan, & Uslu, 2010). A square wave voltammogram and its excitation signal response is shown in **Figure 7** below.

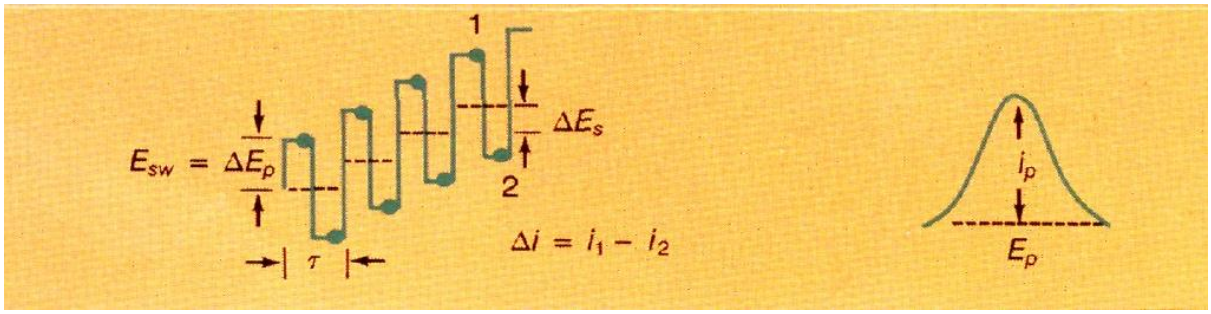

Figure 7: A typical square wave voltammogram (Osteryoung & Osteryoung, 1985).

In SWV the excitation signal consists of a symmetrical square wave pulse of amplitude E_{sw} that is superimposed on a staircase waveform of height ΔE, where the forward pulse of the square wave coincides with the staircase step. The net current is obtained by taking the difference between the forward and reverse currents. The peak height in SWV is directly proportional to the concentration of the electroactive species and the detection limit can be as low as 10^{-8} M (Hussam, 2006).

Application of the AuE/QD Aptasensor towards different concentrations of IFN-γ was carried out in 8 mL of 0.1 M PBS buffer solution, pH 7.4. The SWV was scanned in one direction from -1.0 to 1.5 V. The SWV amplitude of 0.02 V was used with a step potential of 0.004 V and a frequency of 10.0 Hz. The AuE/QD Aptasensor was allowed to stay for 5 min in the electrolyte solution that contained different concentrations of IFN-γ. All SWV measurements were done at room temperature. The electrolyte solution was degassed with nitrogen for at least 15 min before an electrochemical experiment.

3.9.3. Electrochemical Impedance Spectroscopy (EIS)

Electrochemical Impedance Spectroscopy is a powerful technique that investigates the mechanisms of electrochemical reactions by measuring the dielectric and transport properties of materials. This technique is powerful because it is a linear technique that makes the results willingly interpreted in terms of linear systems theory, it is measured over an vast frequency range, the impedance contains all the information from the system by linear electrical perturbations/response techniques, the efficiency is very high and the validity of the data is readily determined using integral transform techniques that are independent of the physical processes involved (Macdonald, 2006).

Impedance spectroscopy is a technique where the sinusoidal perturbation at a certain frequency is applied onto a system and the response is recorded. The process is repeated over a range of frequencies in order for a spectrum to be obtained. In many systems a pseudo potentiostatic measurement is common, the perturbation can be a sinusoidal potential wave of amplitude E_{ac0} superimposed on a constant dc potential E_{dc} and the magnitude and phase of the current density are recorded (Fasmin & Srinivasan, 2017).

EIS data are often interpreted in terms of electrical equivalent circuits (EEC's). The equivalent circuit modelling is to obtain meaningful properties of the system under investigation by modelling the impedance data in terms of an electrical circuit composed of ideal resistors, capacitors and inductors but specialized circuit elements are used because real systems don't behave ideally with processes that occur distributed in space and time. The specialized circuit elements include; the generalized Constant Phase Element (CPE) and Warburg element (Z_w) (Jorcin, Orazem , Pebere, & Tribollet, 2006). The data obtained from EIS can be interpreted from a Nyquist plot and a Bode plot.

The impedance can be illustrated as a vector of length [Z] on the Nyquist plot. In the Nyquist plot the Nyquist is expressed as Z(ω) which is composed of an imaginary part and real part. The imaginary part is plotted on the y-axis and the real part is plotted on the x-axis of a graph. The Nyquist plot along with the equivalent circuit is shown in **Figure 8**; the plot is a semi-circle revealing characteristic of a one-time constant. The low frequency data is on the right side of the plot and the high frequency data on the left side of the plot (Wang, Moser, & Gratzel, 2005).

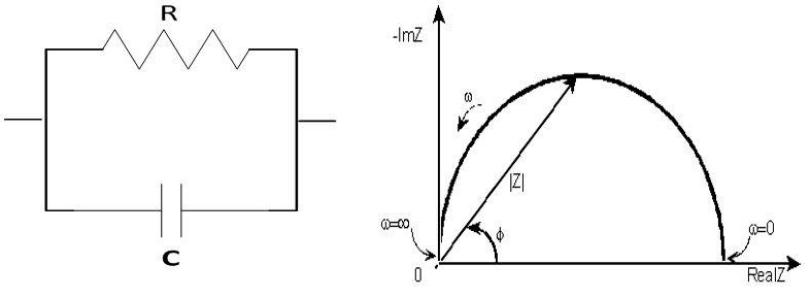

Figure 8: Nyquist plot and equivalent circuit (Jayakumar, Trivedi, Sharma, Rebosura, & Murugesan, 2016).

In the equivalent circuit the resistance represents the conductive pathways for ion and electron transfer, they represent the bulk resistance of material to charge transport, they are also used to represent the resistance to charge transfer processes at the electrode

surface. The capacitors and inductors are related with space-charge polarization regions such as the electrochemical double layer and the adsorption and desorption processes at the surface of the electrodes.

The Bode plot is a plot of the phase and magnitude of a transfer function or quality of complex value frequency. The plot has the phase which is in degrees and magnitude in decibels and it is plotted versus the log frequency. The plot of magnitude is also log-log in nature since its described in the form of decibels and the frequency is also in logarithmic. In the Bode plot the impedance is plotted with log frequency on the x-axis and both the impedance and phase is on the y-axis (He & Mansfeld, 2009). The Bode plot is shown in **Figure 9**.

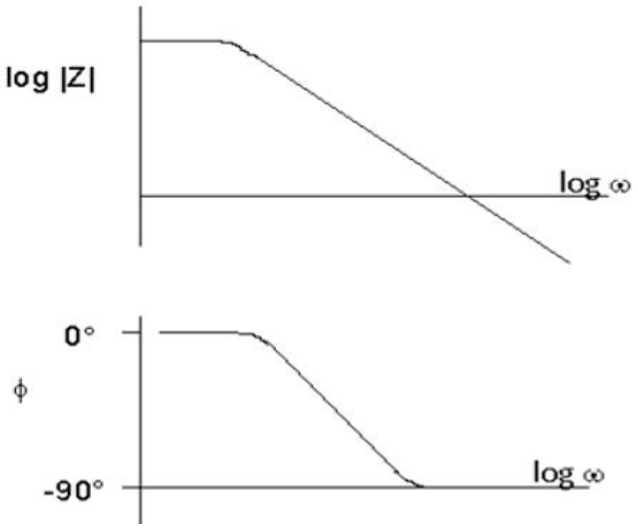

Figure 9: Representation of a Bode plot (Jayakumar, Trivedi, Sharma, Rebosura, & Murugesan, 2016).

The electrochemical properties of the modified and unmodified surface of AuE were studied using EIS. The EIS measurements were carried out in frequency range of 0.1 Hz minimum and $1x10^4$ Hz maximum. EIS was used to study the application of the AuE/L-cysteine-In_3TeSe_2/Aptamer towards different concentrations of IFN-γ in 8 mL of 0.1 M PBS, pH 7.4

within a frequency range of 0.1-1x10^4 Hz. The AuE/L-cysteine-In_3TeSe_2/Aptamer was allowed to stay for 5 min in the electrolyte solution that contained different concentrations of IFN-γ. All EIS measurements were done at room temperature. The electrolyte solution was degassed with nitrogen for at least 15 min prior to an electrochemical experiment. The EIS modelling of the data was done using ZView software.

Chapter 4

Results and Discussion

4.1. Characterization of L-cysteine capped In_3TeSe_2 QD

4.1.1. Ultraviolet-visible spectroscopy (UV-Vis)

UV-Visible spectroscopy provided information on the bandgap energy, particles size and the distribution of the L-cysteine-In_3TeSe_2 QD. The UV-vis spectrum of the L-cysteine-In_3TeSe_2 QD precursors; NaHTe, NaHSe and L-cysteine-$InCl_3$ is displayed in **Figure 10**. Two absorption bands at 215 and 278 nm were observed for NaHTe, one broad absorption band at 265 nm for NaHSe and one absorption band at 250 nm for L-cysteine-$InCl_3$. The Indium chloride capped with L-cysteine absorbed light in the UV region.

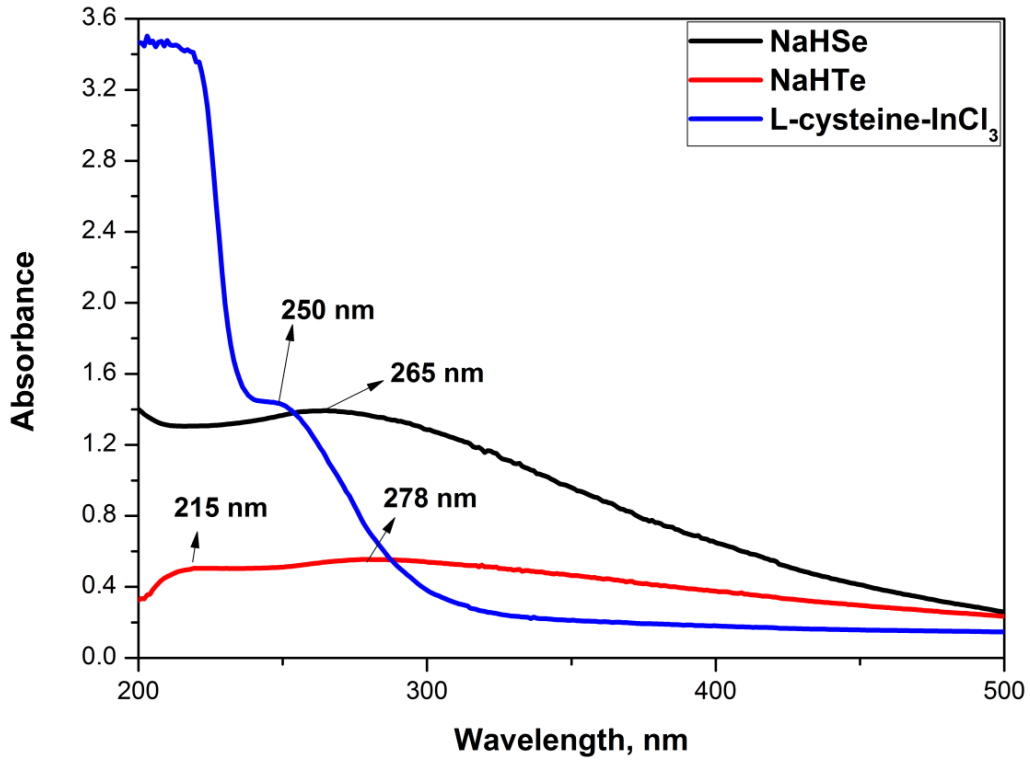

Figure 10: UV-Vis spectrum of NaHSe, NaHTe and L-cysteine-$InCl_3$

The UV-vis spectrum for L-cysteine-In_3TeSe_2 QD is shown in **Figure 11**. A somewhat broad absorption maximum can be seen for the QD at 291 nm. The absorption band broadness can be an indication of a broad size distribution of the L-cysteine-In_3TeSe_2 QD, which due to the broad size distribution the bandgap difference between the different sized particles will be big, resulting in majority of the electrons being excited over a wide range of wavelength (Gullapalli & Barron, 2010) . The bandgap energy of the QD was found to be 3.0 eV, and was calculated using the following formula:

$$\mathbf{E} = \frac{\mathbf{hc}}{\boldsymbol{\lambda}} \qquad (4.1.1.1.)$$

Where E is the bandgap energy, h is Planck's constant, c is the speed of light and λ is the experimental optical absorption wavelength. The bandgap of the QD is an indication of the formation of very small sized particles (nanophase of the material) because according to the effective mass approximation (EMA), as the size of a semiconductor material decreases their bandgap energy increases.

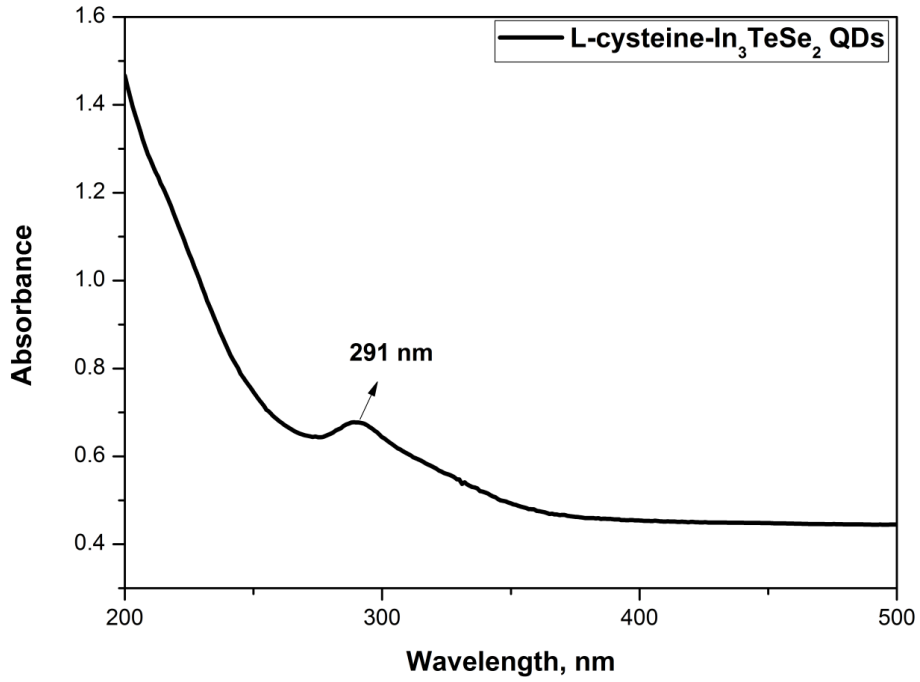

Figure 11: UV-Vis spectrum of L-cysteine-In_3TeSe_2 QD.

4.1.2. Fluorescence Spectroscopy (PL)

The fluorescence spectra of microwave irradiation L-cysteine-In_3TeSe_2 QD is displayed in **Figure 12**. The QD were excited at 290 nm and gave an emission maximum at 321 nm. There are two distinct bands observed in the PL spectra, firstly a strong narrow emission band at 321 nm and secondly a broad band around 400 nm that can be attributed to trap state emission that occur when the QD form rapidly through microwave irradiation. The trap state emission occurs either when there is incomplete capping due to the rapid microwave irradiation process or it could be due to the small size of the nanoparticles having a higher surface to volume ratio and hence higher surface defects which leads to trap states (Kapitonov, Stupak, Gaponenko, Petrov, Rogach, & Eychmuller, 1999), (Rogach, et al., 2007).

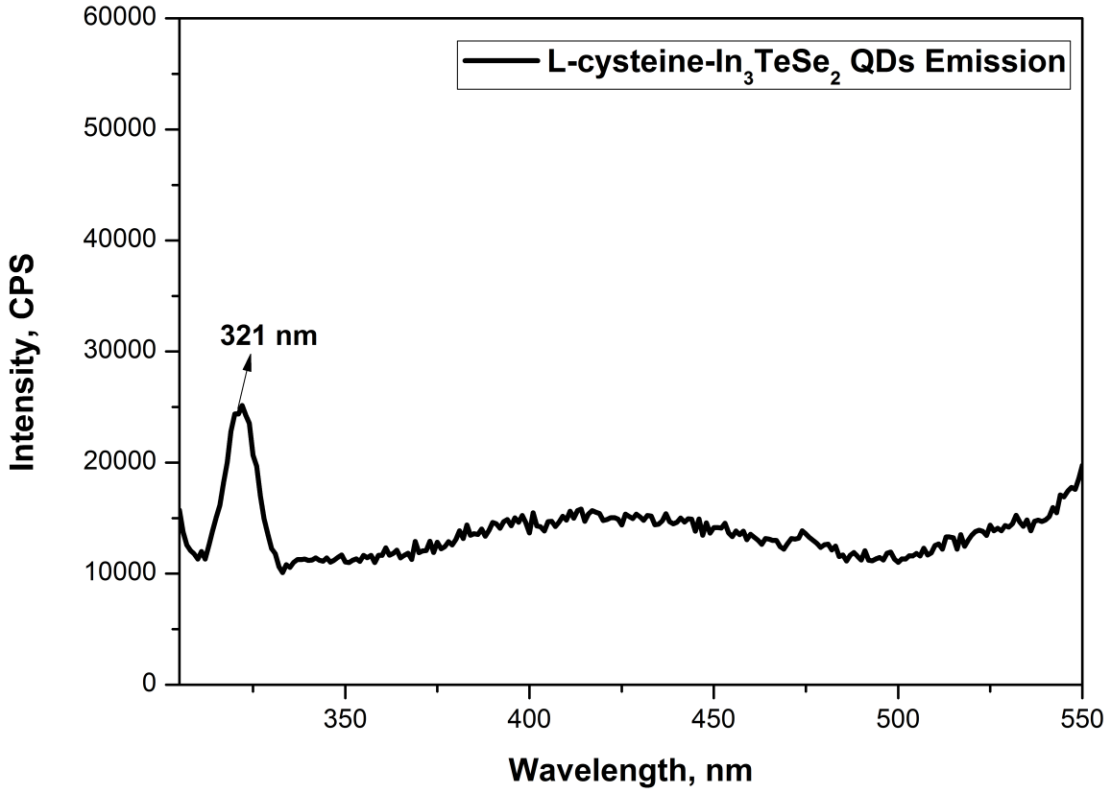

Figure 12: Fluorescence emission spectre of L-cysteine-In_3TeSe_2 QD

4.1.3. Fourier Transform Infrared Spectroscopy (FTIR)

The Fourier Transform Infrared (FTIR) Spectrum for L-cysteine and L-cysteine capped In_3TeSe_2 QD is revealed in **Figure 13**. The spectrum for pure L-cysteine has a characteristic stretching vibration band at 2550 cm^{-1} which is attributed to the S-H group and another absorption band at 2080 cm^{-1} which is due to the N-H group of the NH_3^+ group of L-cysteine. Both bands disappear; the S-H band disappears due to the cleavage of S-H bonds and formation of In_3-S bonds indicating that the thiol of L-cysteine has successfully combined on the surface of the In_3TeSe_2 QD, the disappearance of the N-H band is due to the basification of the NH_3^+ group of L-cysteine during the synthesis procedure (Li, Liao, Ding, & Zeng, 2017).

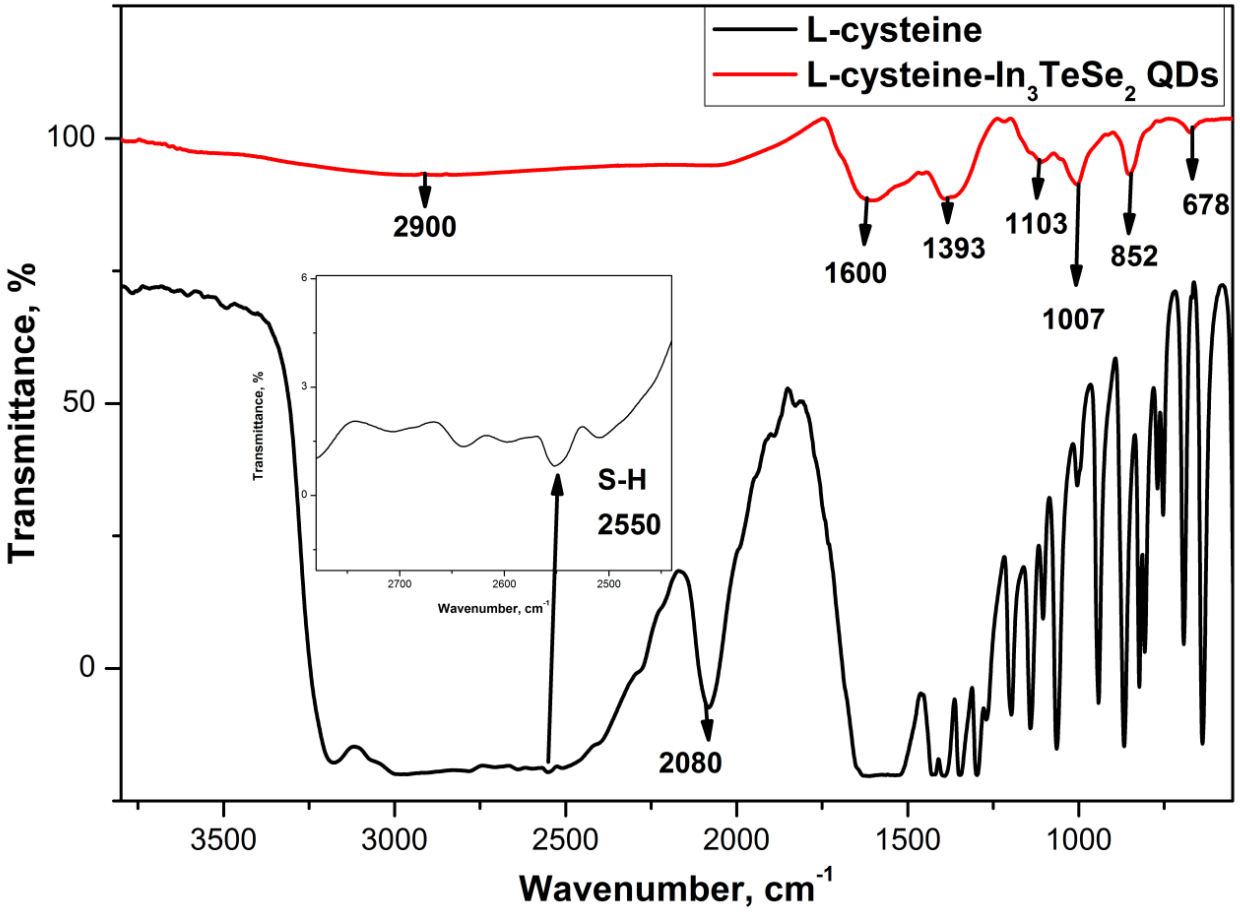

Figure 13: FTIR spectrum of L-cysteine and L-cysteine-In_3TeSe_2 QD.

The spectra for L-cysteine capped In_3TeSe_2 exhibits well defined bands. The broad band at 2900 cm^{-1} is due to the OH, COOH group from the capping agent L-cysteine, the medium absorption band at 1600 cm^{-1} corresponds to the C=O vibration representing the carboxyl group, the medium band at 1393 cm^{-1} represents the C-O-H bend and the band at 1103 cm^{-1} arises from the medium stretch vibration of the C-O bond from the capping agent. The medium stretching vibration at 1007 cm^{-1} relates to the C-N bond, the strong absorption band at 852 cm^{-1} correlates to the C-S bond and the weak absorption band at 678 cm^{-1} is due to the N-H bond. There are IR absorption bands that are coexisting of $–COO^-$ and N-H witnessed on both L-cysteine and L-cysteine capped In_3TeSe_2 QD, thus carboxylic acid and amino group are present on the surface of the In_3TeSe_2 QD (Koneswaran & Narayanaswamy, 2009) while the S-H group vibration at 2550 cm^{-1} is absent on the surface of the QD. The absence of the S-H bond and the presence of other bonds that are mentioned above prove the successful capping of the In_3TeSe_2 QD by L-cysteine.

4.1.4. High Resolution Transmission Electron Microscopy (HRTEM)

The shape, size and structure of the L-cysteine capped In_3TeSe_2 were observed with HRTEM micrographs, as shown in **Figure 14** below. The images show that the L-cysteine capped In_3TeSe_2 QD is highly spherical, aggregated and have an average diameter of 6 nm. This is in accordance with information derived from the UV-Vis absorption spectrum, i.e. the formation of very small particles accounting for the high bandgap energy. The elemental composition of the L-cysteine capped In_3TeSe_2 QD were studied using energy dispersive x-ray (EDX) spectroscopy and it revealed that the most abundant elements are In, Te and Se, as displayed in **Figure 15**. The presence of Cu in the spectra is a result of the copper grid that was used to place the sample on. The carbon (C), sulphur (S) and oxygen (O) that are also present in the spectra is a result of the capping agent L-cysteine. Furthermore the Na

that is present in the spectra results from the reducing agent $NaBH_4$ that was used to synthesise NaHTe and the Sc that is visible in the spectra is a contaminant that was present.

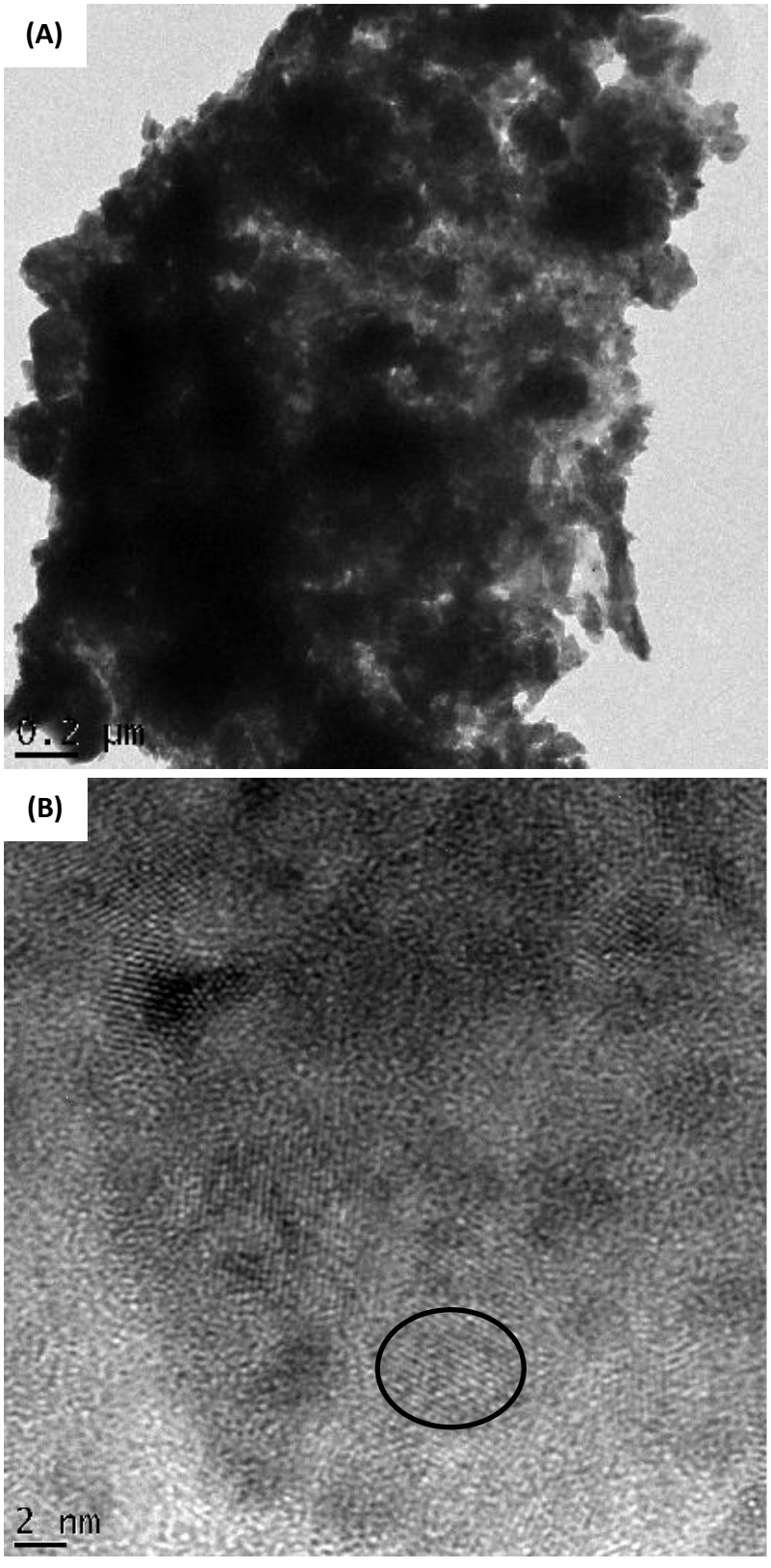

Figure 14: HRTEM micrographs of L-cysteine-In_3TeSe_2 QD a) 0.2 μm and b) 2 nm scale view.

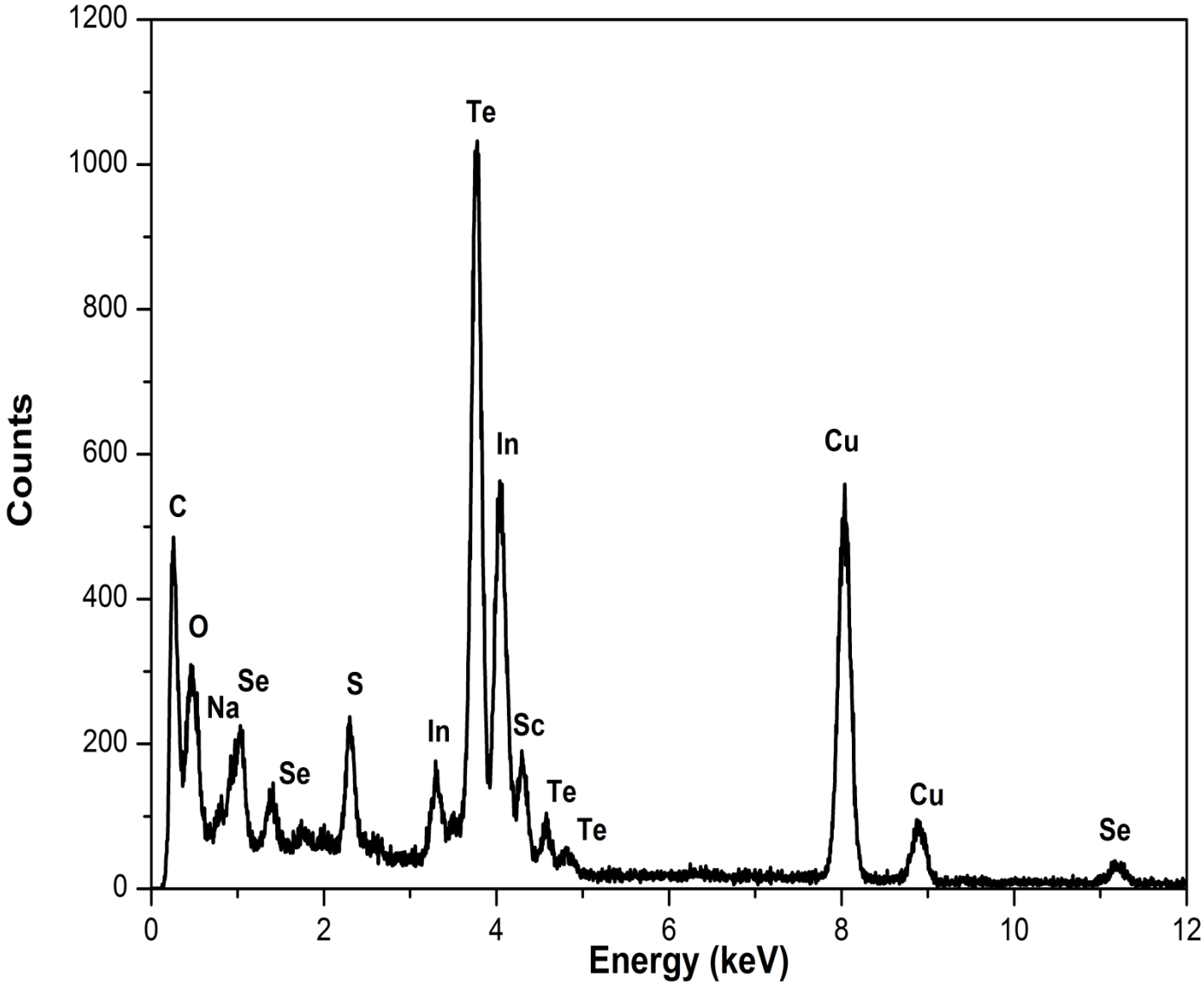

Figure 15: HRTEM Energy Dispersive X-ray (EDX) spectrum of L-cysteine-In_3TeSe_2 QD.

4.1.5. High Resolution Scanning Electron Microscopy (HRSEM)

The HRSEM micrographs are displayed in **Figure 16** below; it provided information on the morphology and composition of the L-cysteine capped In_3TeSe_2 QD. It was observed that the QD appeared to be highly spherical nanocrystals aggregated together, the aggregation may be due to the fact that too little capping agent was used or it could be because L-cysteine is water soluble molecule and when capping the quantum dot it made the quantum dot water soluble and water soluble QD tend to aggregate (Liu, Wang, & Li, 2009).

The elemental composition of the L-cysteine capped In_3TeSe_2 QD was studied by EDX spectroscopy and is displayed in **Figure 17**. The EDX spectra of HRSEM and HRTEM are in

correlation with each other except the addition of Cl in the HRSEM EDX spectra which is due to the starting material of $InCl_3$; also no copper is seen in the HRSEM EDX spectra, this is because carbon tape was used for the sample analysis instead of a copper grid. The stoichiometric formula of the synthesized quantum dots were calculated using the atomic ratios provided from the HRTEM and HRSEN EDX spectre.

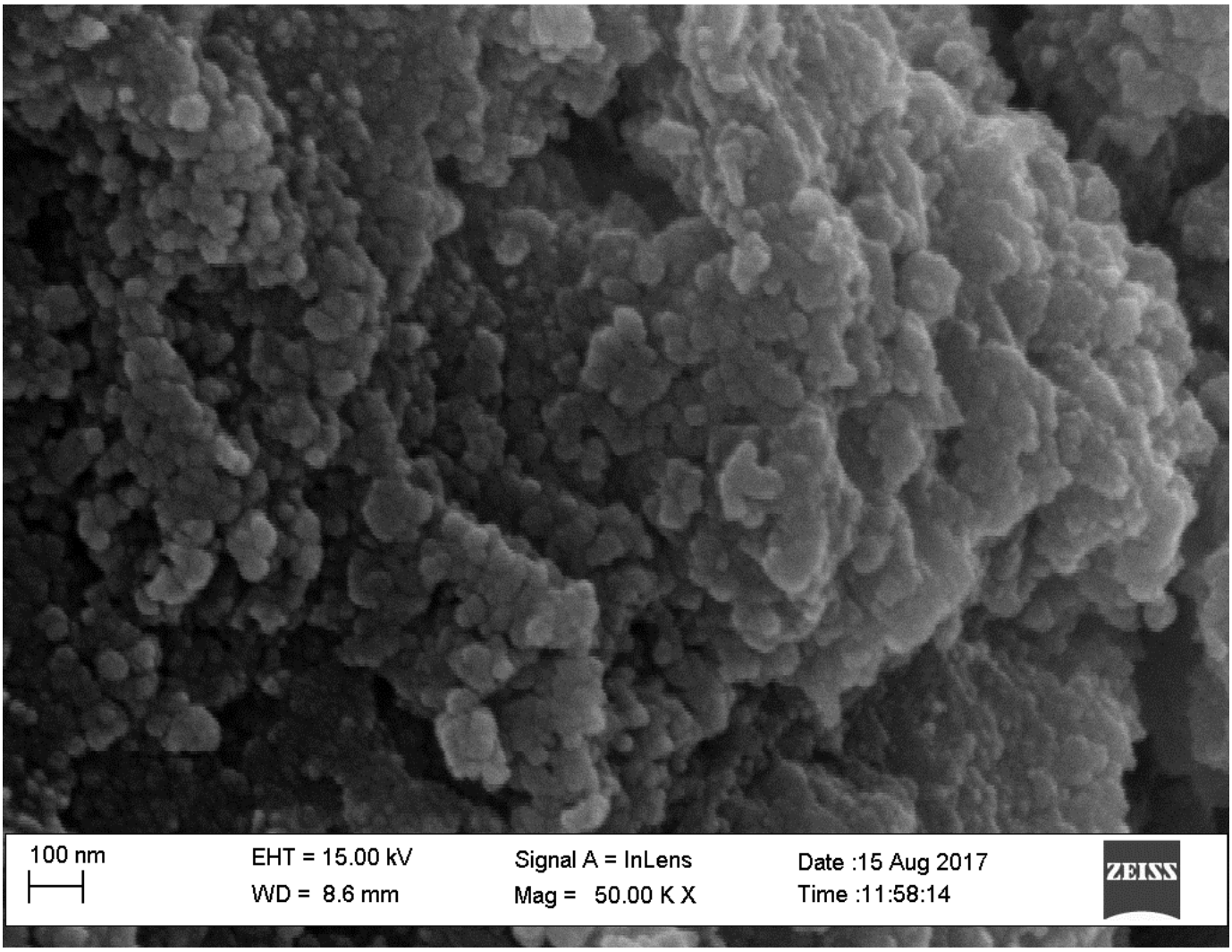

Figure 16: HRSEM micrographs of L-cysteine-In_3TeSe_2 QD at 100 nm scale view.

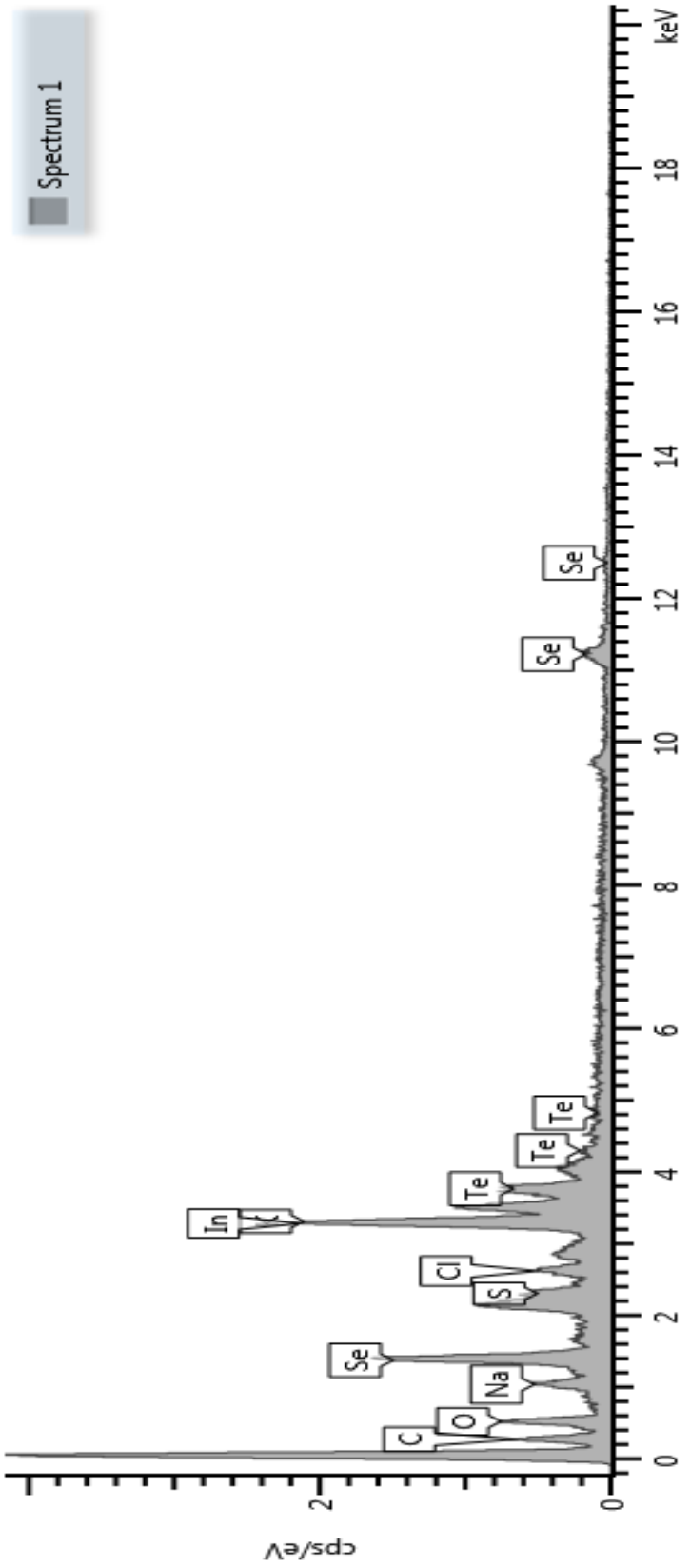

Figure 17: HRSEM Energy Dispersive X-ray (EDX) spectrum of L-cysteine-In_3TeSe_2 QD.

4.1.6. Small- angle X-ray Scattering (SAXS)

The Small Angle X-ray Scattering (SAXS) provided more information on the size and shape of the L-cysteine capped In_3TeSe_2 QD. The shape of the QD is displayed in the pair-distance distribution function (PDDF) model in the inset of **Figure 18** below. The PDDF plot shows a symmetrical peak at 25 nm followed by a second peak at 55 nm, this means that the particles are spherical in shape but are agglomerated, the hump at 55 nm indicates that the particles are agglomerated. The accurate size of the QD is displayed in the size by number plot in **Figure 18** as well. The plot displays a peak at 6 nm meaning that the majority of the particles have an average diameter of 6 nm in size with the other peaks at 21 nm and 33 nm being the agglomerated particles. These results are in accordance with the HRTEM analysis that reported the average diameter of the QD at 6 nm.

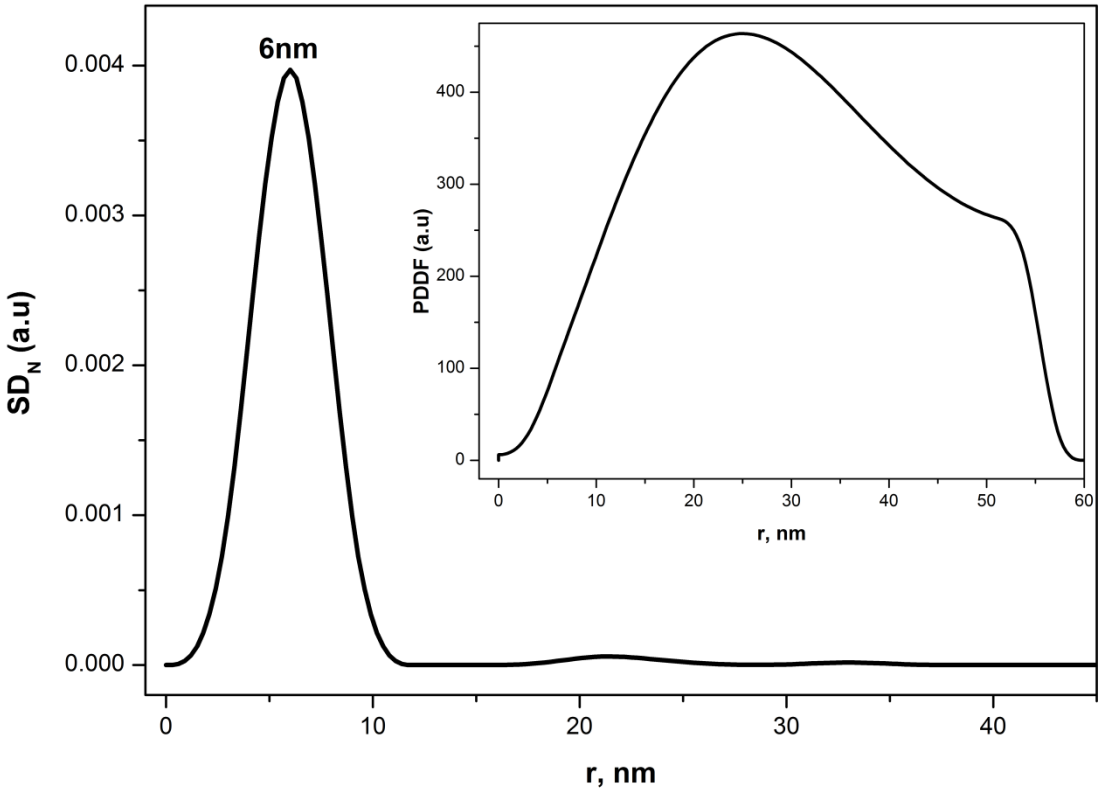

Figure 18: SAXS particle size by number plot and corresponding PDDF plot (inset) of L-cysteine-In_3TeSe_2 QD

4.1.7. Cyclic Voltammetry (CV)

Cyclic voltammetry was used to study the electrochemical properties of the L-cysteine capped In_3TeSe_2 QD, however before this was done the precursors of L-cysteine-In_3TeSe_2 QD were first studied. This study was done to see whether the new peaks that are observed were due to the adsorbed QD. **Figure 19 (A), (B)** and **(C)** shows the cyclic voltammograms of AuE/L-cysteine-$InCl_3$ versus bare AuE, NaHTe and NaHSe. In **Figure 19 (A)** the cyclic voltammograms of AuE/L-cysteine-$InCl_3$ and bare AuE is seen. In the bare Au electrode two peaks are seen, the anodic peak at 1.13 V and a cathodic peak at 0.41 V, as for the L-cysteine-$InCl_3$ voltammogram two anodic peaks and one cathodic peak is visible, a shoulder peak A_1 at 0.6 V, a strong wide peak A_2 at 0.86 V and a cathodic peak C_1 at -0.70 V. The shoulder peak at A_1 could be due to the oxidation of L-cysteine to cystine while the broad peak at A_2 could be due to the later oxidation of cystine (Pereira, Vazquez, Deban, & Aller, 2013). The reduction peak at C_1 could be due to the reduction of In^{3+} to In reduction of Indium ions on the surface of the electrode has been reported before (Chung & Lee, 2012) however there might be a shift in some of the peaks depending on how basic or acidic the electrolyte solution is. In **Figure 19 (B)** the cyclic voltammagram of NaHTe is presented, it shows three anodic peaks and two cathodic peaks, a broad peak A_1 at -0.18 V, a strong sharp peak A_2 at 0.38 V and a shoulder peak A_3 at 0.51 V. The cathodic peak C_1 at -0.14 V and a weak peak C_2 at -0.64 V are also visible. The oxidation peak at A_1 could be due to the oxidation of Te^0 to $Te^{2+,}$ the peak at A_2 could be due to the oxidation of Te^{2+} to Te^{4+} while the peak at A_3 could be due to the oxidation of Te^{4+} to Te^{6+} state. The reduction peaks of C_1 and C_2 could be due to the reduction of Te which generates Te^0 at C_1 and Te^{2-} at C_2. In **Figure 19 (C)** the cyclic voltammagram for NaHSe is shown two anodic and two cathodic peaks are observed, a weak peak A_1 at 0.36 V, a medium peak A_2 at 0.61 V, when the potential is

swept in the negative direction you get a peak C_1 at 0.04V and another weak broad peak C_2 at -0.56 V.

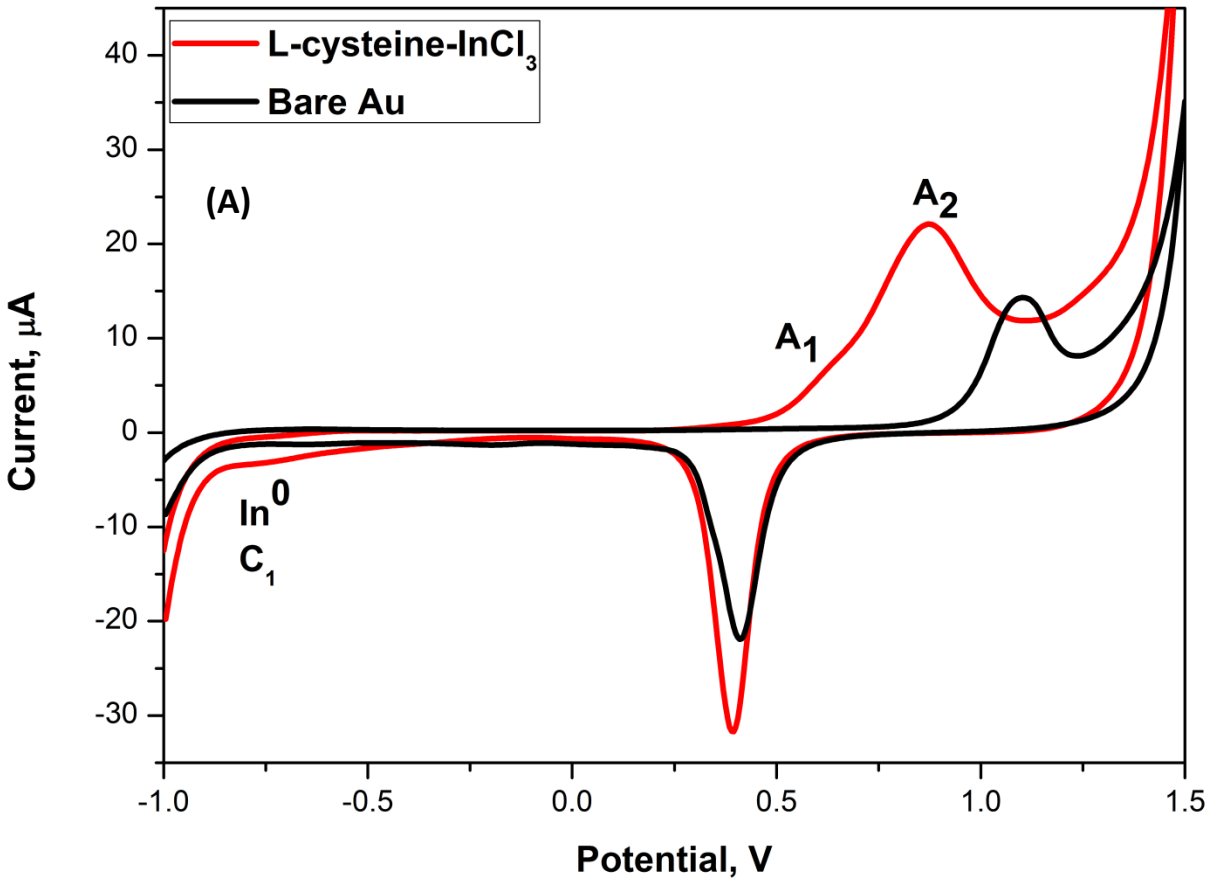

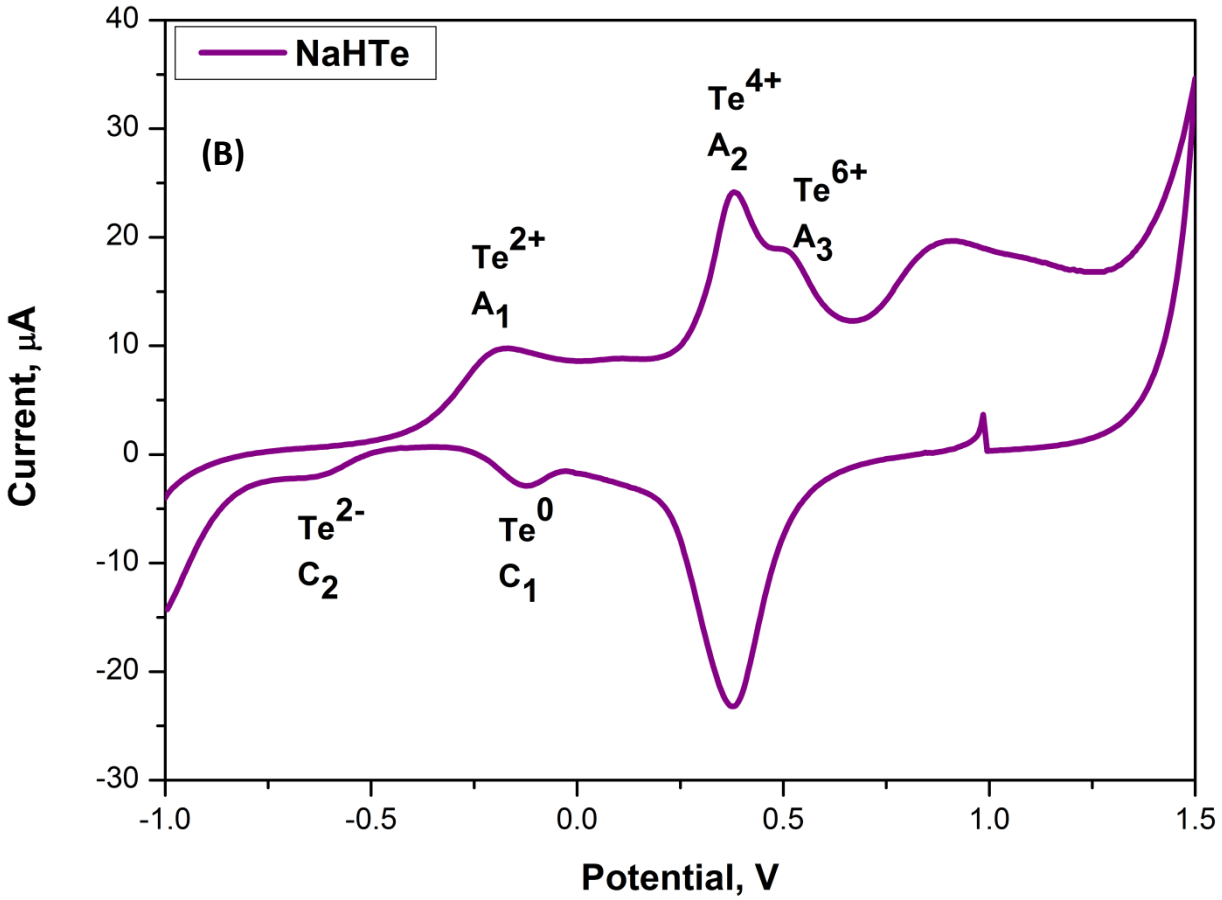

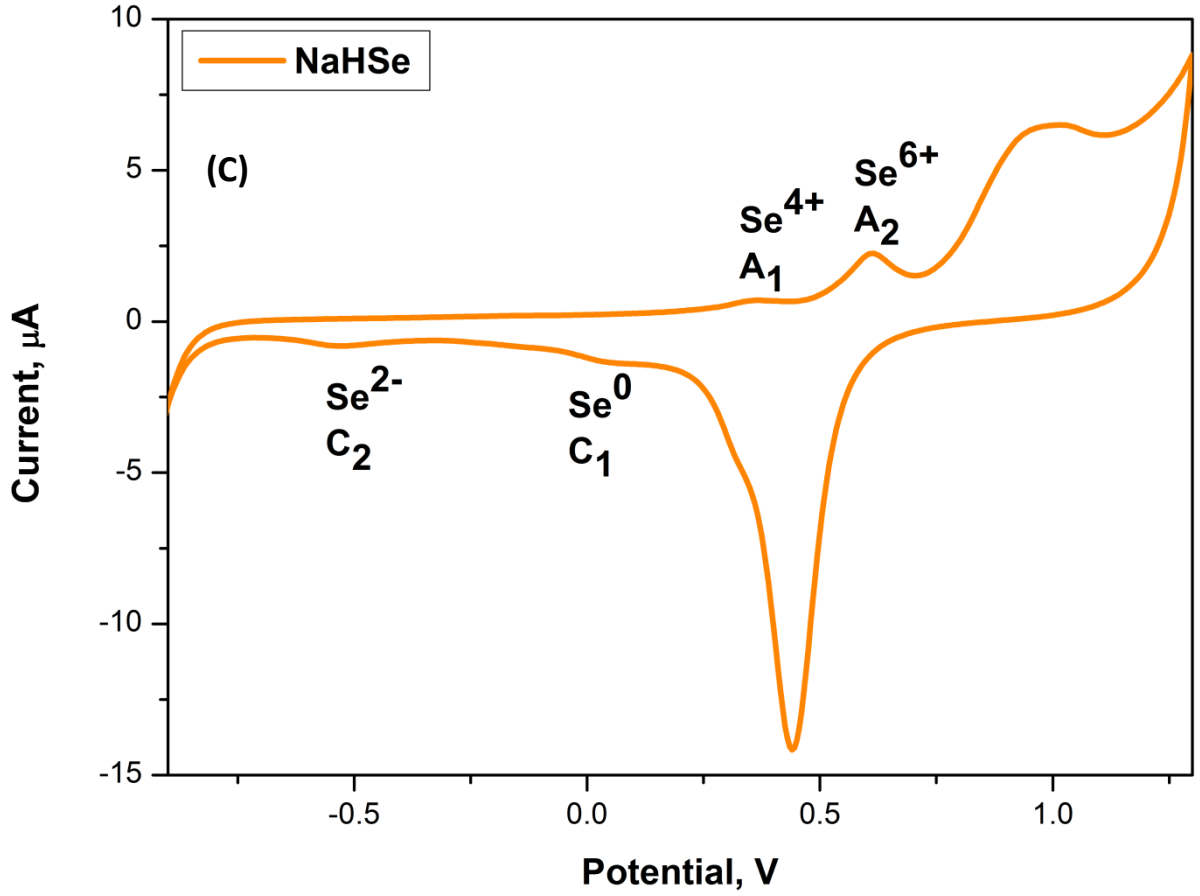

Figure 19: Cyclic voltammograms of a) L-cysteine-$InCl_3$ versus bare AuE, b) NaHTe and c) NaHSe in 0.1 M PBS, pH 7.4 at 0.1 V/s.

Cyclic Voltammetry was used to study the electrochemical properties of L-cysteine capped In_3TeSe_2 QD. **Figure 20** shows the cyclic voltammagrams of bare AuE and modified AuE/L-cysteine-In_3TeSe_2 QD. Four anodic peaks and three cathodic peaks are observed, peak A_1 at 0.28 V, a shoulder peak A_2 at 0.36 V, a strong peak A_3 at 0.48 V and a broad peak A_4 at 0.78 V. When running potential in the negative direction three cathodic peaks were observed, peak C_1 at -0.09 V, weak broad peak C_2 at -0.48 V and lastly peak C_3 at -0.69 V. The peak at A_1 is attributed to the oxidation of the QD which then generates Te^{4+}, the peak at A_2 and A_3 is due to oxidation of the QD that generates Se^{4+} and Te^{6+} the peak at A_3 is also due to surface defects of Te dangling bonds on the surface of the nanocrystal (Matos, Candido, Souza Jr, da Costa, Sussuchi, & Gimenez, 2016). The broad peak at A_4 is due to the oxidation

of the capping agent to cystine. The cathodic peak C_1 is due to reduction of Te^{6+} to Te^0 and Se^{4+} to Se^0 and peak C_2 is due to reduction of Te^0 to Te^{2-} and Se^0 to Se^{2-}. The last peak at C_3 is attributed to the reduction of In^{3+} to In^0 however this peak overlaps with the reduction of Te and Se species. The overlapping of peaks results in In-Te-Se interactions. The oxidation and reduction peaks of the QD all has a negative shift towards lower potentials when compared to the peaks of the individual precursors that are found in the same region of peak potentials, this is due to electron confinement in three dimensions which intern enhances the electrochemical reaction. The QD lower the activation energy of the reaction which causes a shift toward lower oxidative and reductive potentials, signifying a faster reaction.

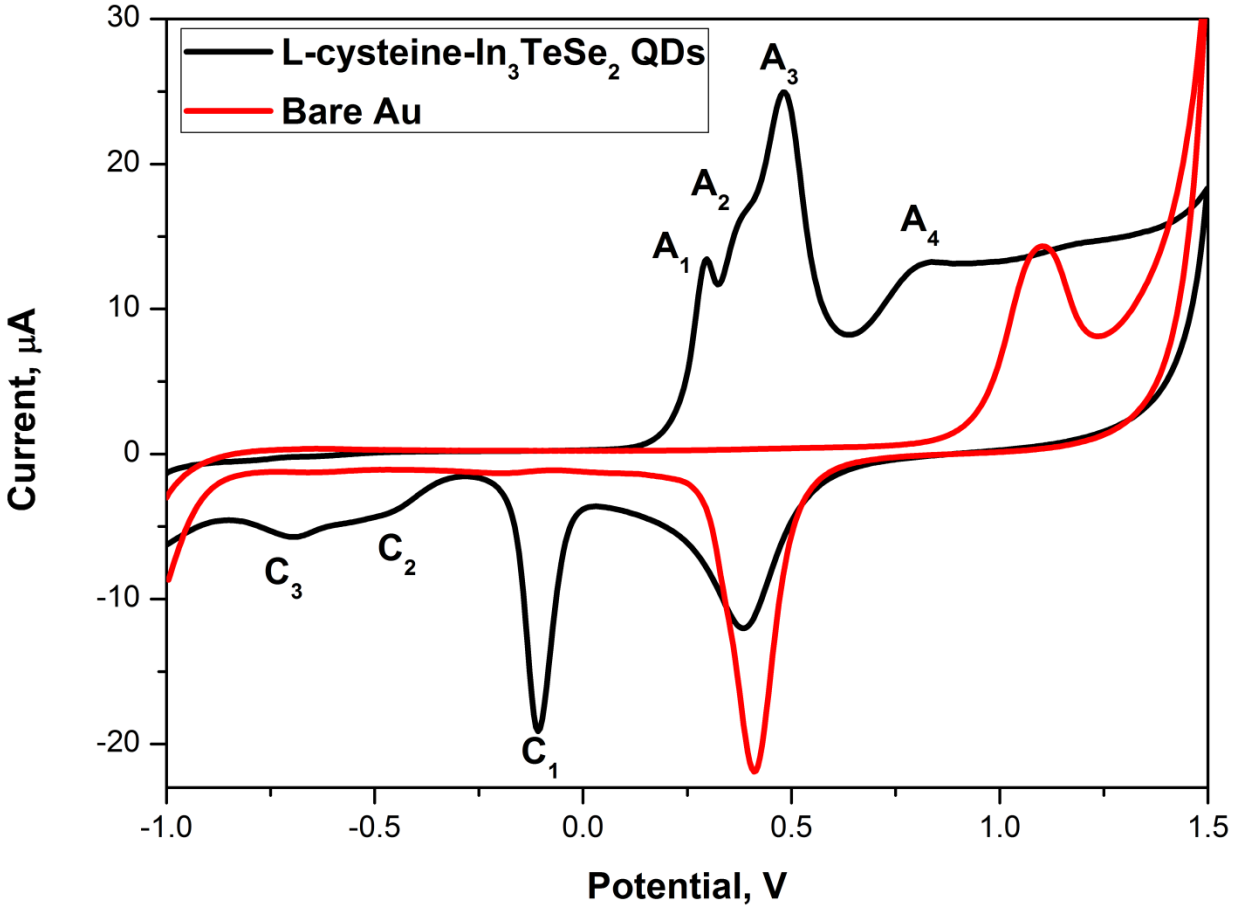

Figure 20: Cyclic voltammograms of Bare AuE and AuE/L-cysteine-In_3TeSe_2 QD in 0.1 M PBS, pH 7.4 at 0.1 V/s.

Figure 21 displays a multi-scan of the L-cysteine-In_3TeSe_2 QD and it can be seen that as the scan rate increases the anodic peaks shifts to more positive potentials while the cathodic peaks shifts to more negative potentials; this is an indication of slow electron transfer processes and kinetic effects (Matos, Candido, Souza Jr, da Costa, Sussuchi, & Gimenez, 2016). Se and Te surface state defects are evident in the L-cysteine capped In_3TeSe_2 QD, which is why a high number of oxidizable Te and Se defects are found in the QD.

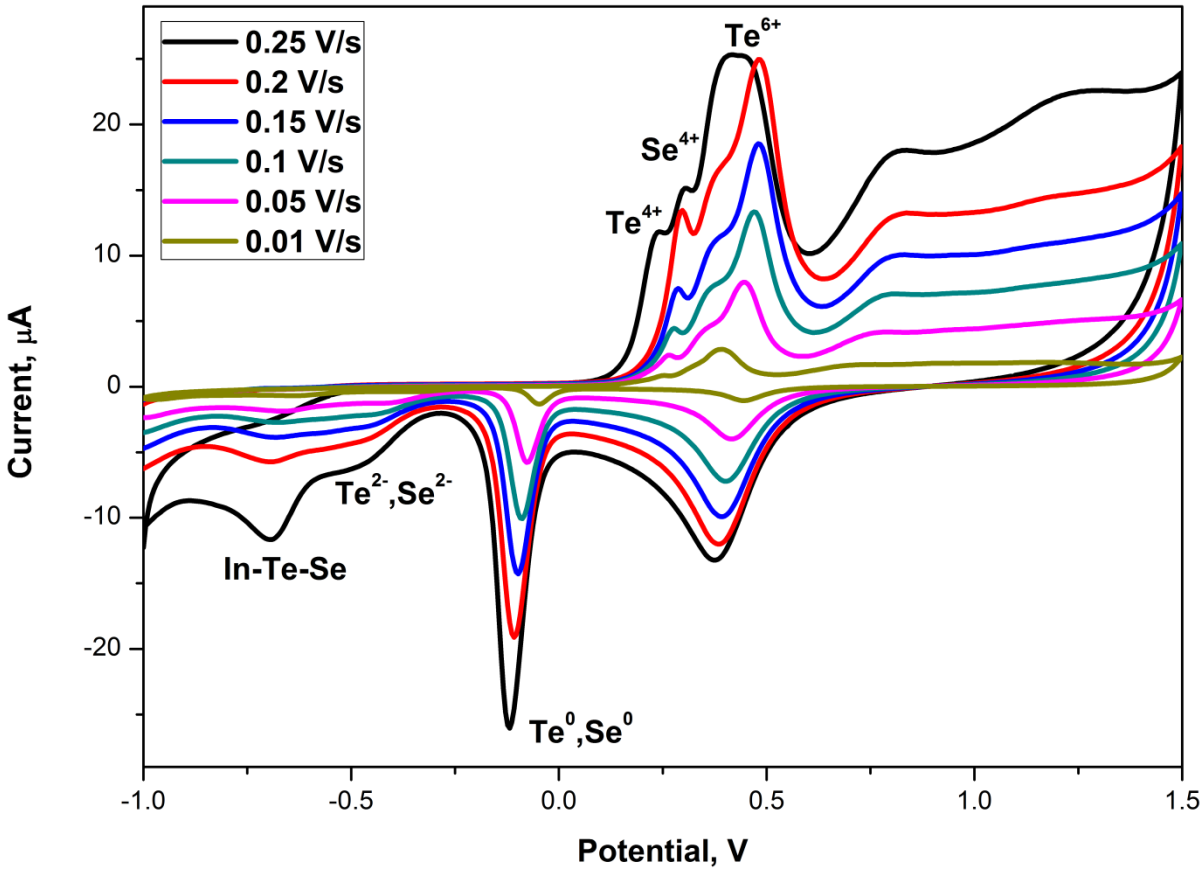

Figure 21: Multi-scan voltammograms of AuE/L-cysteine-In_3TeSe_2 QD in 0.1 M PBS, pH 7.4 at 0.01-0.25 V/s.

A close study of anodic peak A_3 was performed by constructing a plot of peak current ($I_{p,a}$) versus scan rate between 0.01-0.2 V/s to obtain additional information on the redox reactions of the QD as illustrated in **Figure 22**. It is observed that the peak current increases linearly with scan rate with a linear correlation coefficient of R^2 of 0.998, indicating the

electrochemistry of adsorbed quantum dot on the surface of the bare Au electrode which is further observed in the peaks in **Figure 21**.

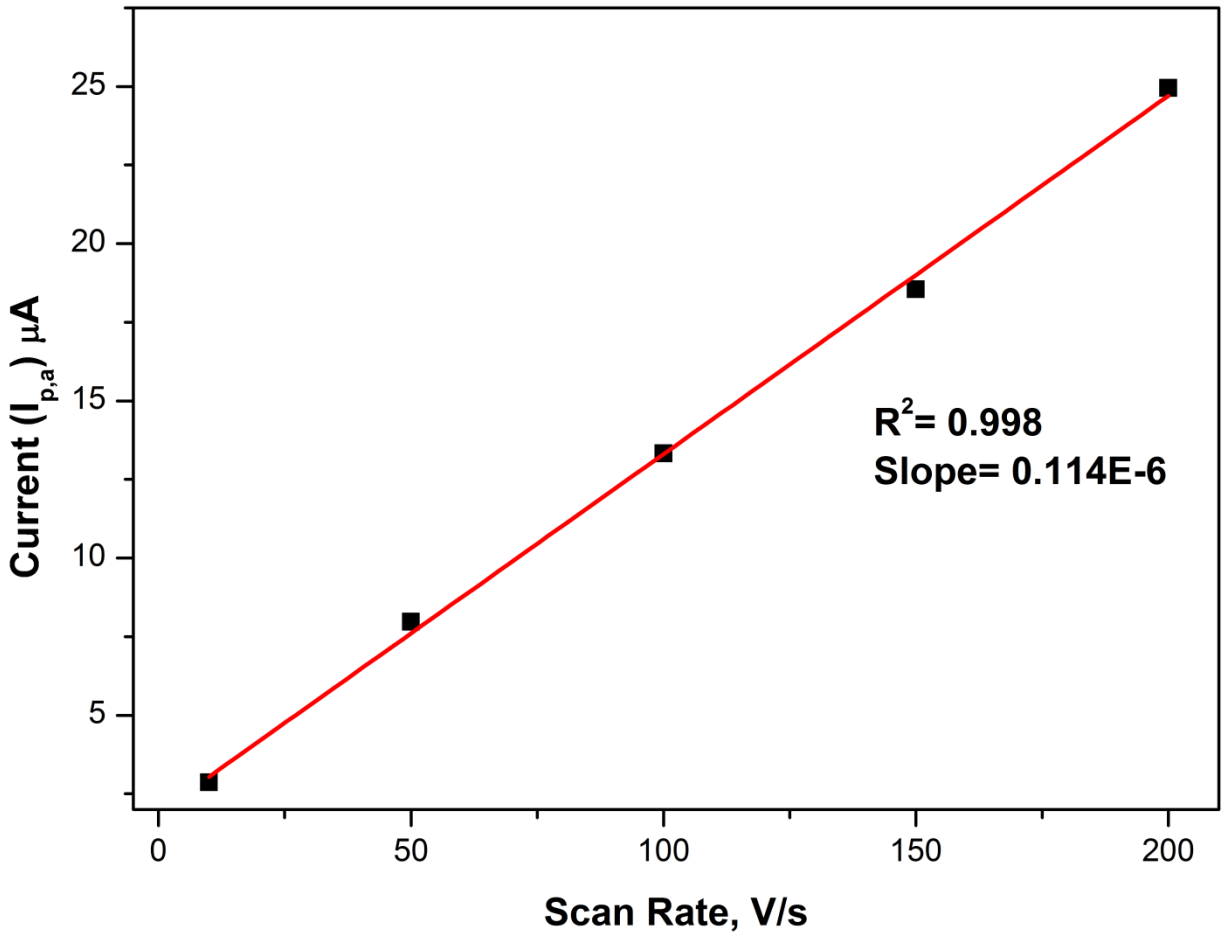

Figure 22: Anodic (peak A_3) plot of peak current ($I_{p,a}$) versus scan rate(v).

Since the electrochemical reaction is controlled by adsorption, the surface concentration of the adsorbed L-cysteine-In_3TeSe_2 QD on the surface of the Au electrode could be determined by using the Brown Anson approximation given below.

$$I_{p,a} = \frac{n^2F^2A\Gamma}{4RT} V \qquad (4.1.7.1)$$

where $I_{p,a}$ = peak current in A, n = 1 number of electrons, F = 96485 C mol^{-1} (faradays constant), A = 0.0201 cm^2 geometric area of the electrode, R = 8.314 J mol^{-1} K^{-1} (gas constant), T = 298.15 K (absolute temperature) and v = scan rate in V s^{-1} and Γ = surface concentration coverage in $mol.cm^2$. Hence the surface concentration of the surface adsorb QD was calculated to be $\Gamma = 8.15\times10^{-4}$ $mol.cm^{-2}$.

4.1.8. Electrochemical Impedance Spectroscopy (EIS)

The electrocatalytic properties of the L-cysteine-In_3TeSe_2 QD were studied by EIS, and the data obtained was explained using Nyquist and Bode plots. The Nyquist plot of bare AuE and AuE/L-cysteine-In_3TeSe_2 QD are shown in **Figure 23.** The Nyquist plots were interpreted according to the equivalent circuit model which is displayed in **Figure 24**. The circuit consists of solution resistance (R_s), constant phase element (CPE) which describes the double layer capacitance properties and lastly the electron transfer resistance (R_{ct}). From this equivalent circuit model the charge transfer resistance of bare AuE was $2.6x10^6$ Ω while the charge transfer resistance for AuE/L-cysteine-In_3TeSe_2 QD was $5.5x10^5$ Ω. The charge transfer resistance for bare Au electrode was bigger than the charge transfer resistance for the AuE/L-cysteine-In_3TeSe_2 QD, this greater charge transfer resistance that was obtained for the bare Au electrode indicates that the charge transfer speed was slower. The charge transfer speed for the QD were faster because of the QD having less charge transfer resistance indicating that it is a better charge conducting material.

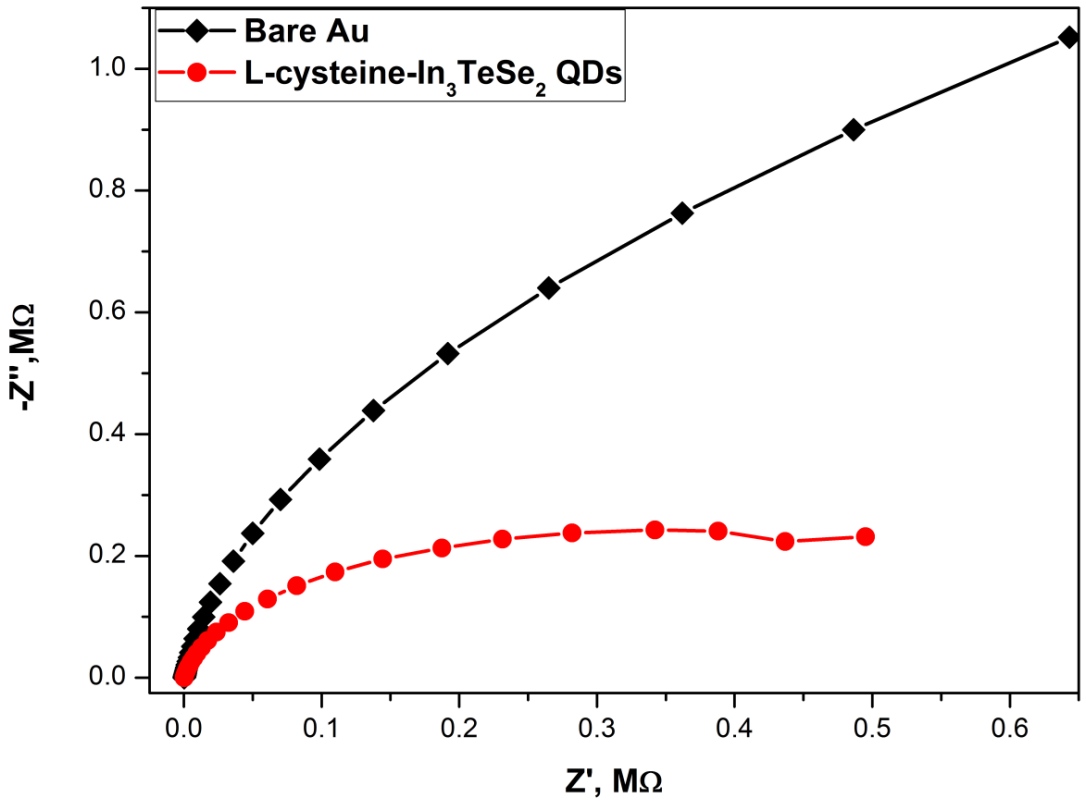

Figure 23: Nyquist plot of bare AuE and AuE/L-cysteine-In_3TeSe_2 QD in 0.1 M PBS, pH 7.4.

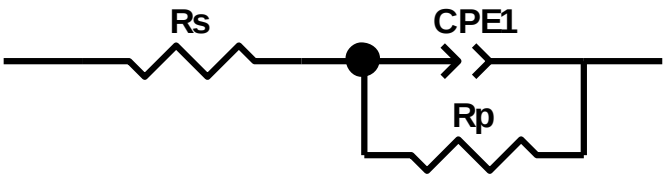

Figure 24: Randles equivalent circuit used to model impedance date of bare AuE and L-cysteine-In_3TeSe_2 QD in 0.1 M PBS, pH 7.4.

The Bode plot representing the frequency dependence of both the impedance and the phase angle of the bare AuE and AuE/L-cysteine-In_3TeSe_2 QD is displayed in **Figure 25** below. It was observed that as the frequency increased the impedance of both the bare AuE and the QD decreased, however at lower frequencies there was in increase in impedance for the bare AuE and the QD. At low frequencies the AuE/L- cysteine-In_3TeSe_2 QD displayed a lower phase angle of 25˚ compared to the 58˚ of the L-cysteine-In_3TeSe_2/AuE QD. These results

indicate a decrease in conductivity of the L-cysteine-In_3TeSe_2/AuE system. Even though the phase angle of the QD has a lower phase angle (25˚) it is still within the range of values for a typical semiconductor material. The results obtained from both the Nyquist plot and Bode plot are in accordance with each other.

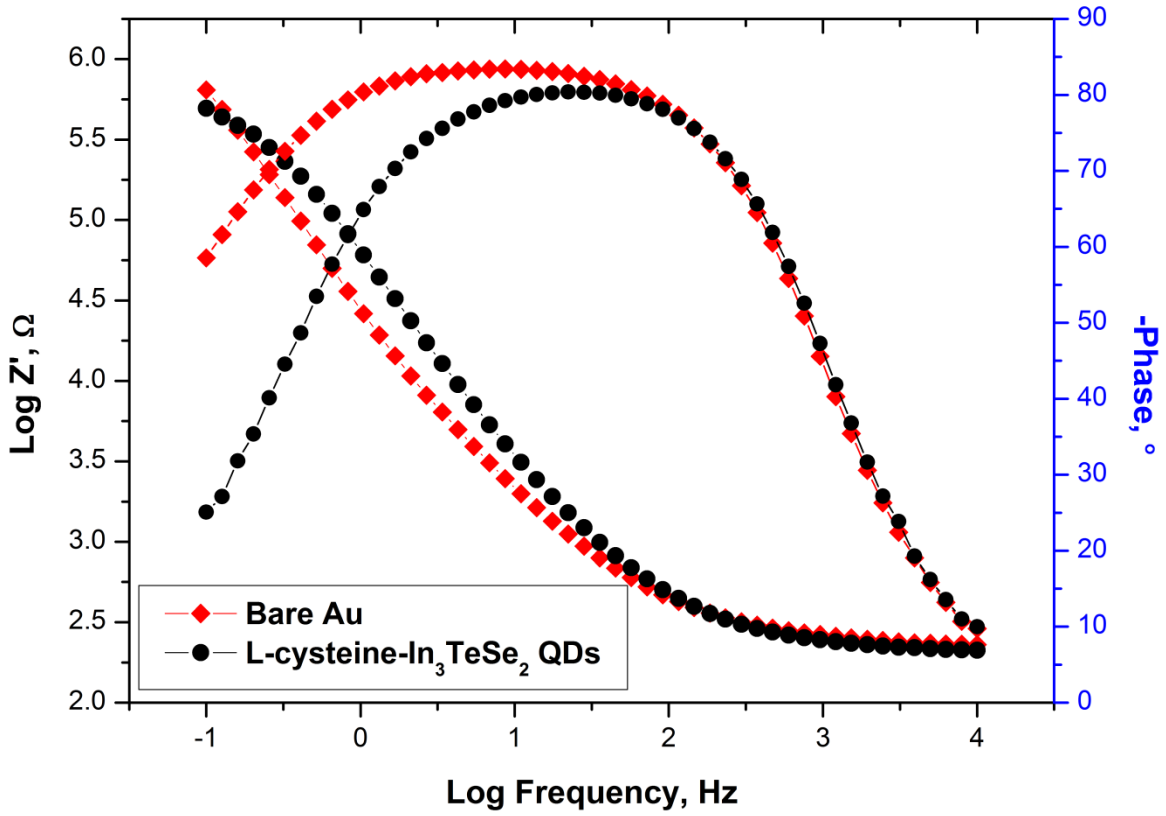

Figure 25: Bode plots of bare AuE and AuE/L-cysteine-In_3TeSe_2 QD in 0.1 M PBS, pH 7.4.

4.2. Characterization of L-cysteine-In_3TeSe_2 QD based Aptasensor

4.2.1. Cyclic Voltammetry

Cyclic voltammetry and Electrochemical impedance spectroscopy was used for confirmation of the electrode fabrication processes involving the QD aptasensor. The response dynamics of these electrochemical characterization techniques indicated the change in surface area, current and change in resistance, also providing added information about the electrode surface modification (Lee, Wu, Su, Hung, & Hsieh, 2013). The cyclic voltammograms for AuE/L-cysteine-In_3TeSe_2 QD and AuE/L-cysteine-In_3TeSe_2/Aptamer is displayed in **Figure 26** below. The cyclic voltammogram reveals that there was a significant reduction in the anodic peak currents and a less significant reduction in cathodic peak currents when the Aptamer was introduced into the AuE/L-cysteine-In_3TeSe_2 QD system. This could be due to the slow diffusion of electrons of an equilibrium mixture of the Aptamer that's bound to the electrode surface. The two cathodic peaks of the L-cysteine QD at -0.48 V and -0.69 V overlaps with each other and makes one peak at -0.6 V in the AuE/L-cysteine-

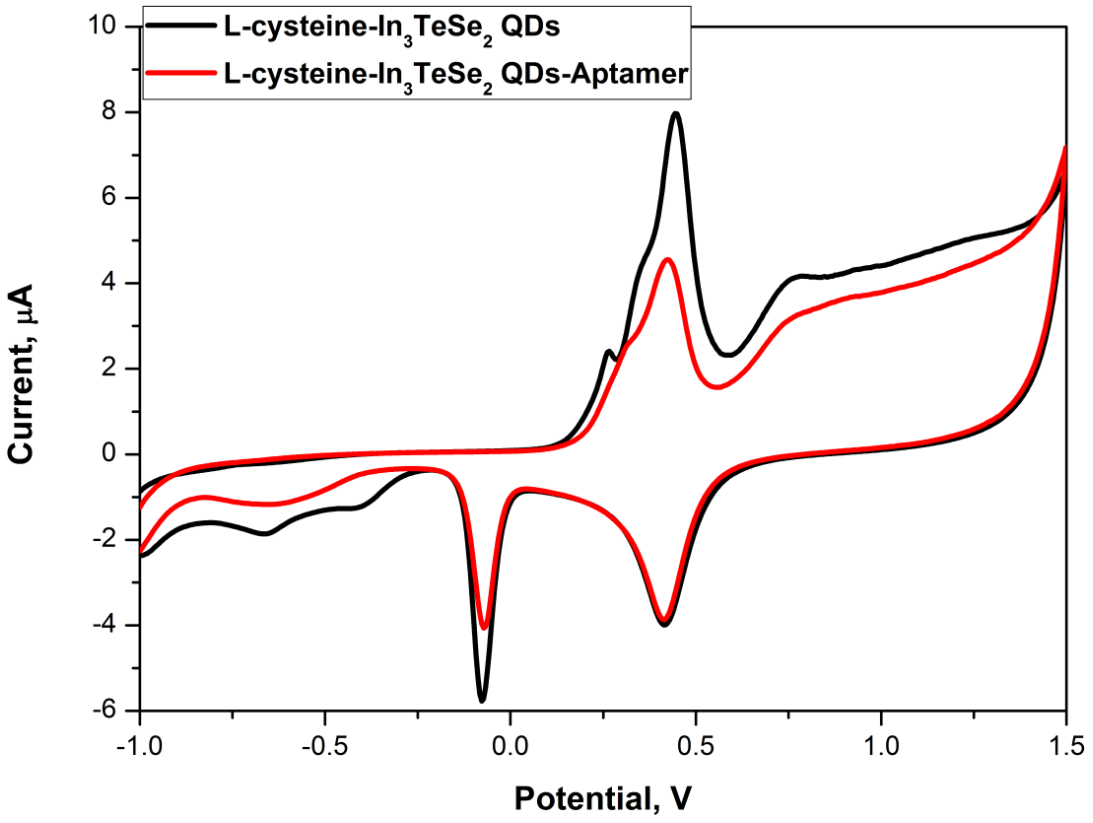

Figure 26: Cyclic voltammograms of L-cysteine-In_3TeSe_2 QD and AuE/L-cysteine-In_3TeSe_2 QD/Aptamer in 0.1 M PBS, pH 7.4 at 0.04 V/s.

In_3TeSe_2/Aptamer cyclic voltammogram. The cathodic peaks of the AuE/L-cysteine-In_3TeSe_2/Aptamer cyclic voltammogram shift to more positive potentials showing that the Aptamer was adsorbed to the surface of the AuE/L-cysteine-In_3TeSe_2 QD.

4.2.2. Electrochemical Impedance Spectroscopy

The Nyquist and Bode plot of the stepwise fabrication of the aptasensor is shown in **Figure 27** and **Figure 28** below. The Nyquist plot was interpreted by fitting the Randles equivalent circuit that was shown in **Figure 24** above. The values obtained at different steps of the aptasensor fabrication are shown in **Table 1** and **Table 2** below. By studying the Nyquist plot after each incubation step it was observed that the AuE/L-cysteine QD-EDC/NHS-Streptavidin/Aptamer has the highest charge transfer resistance (R_{ct} = 3.23x10^6 Ω) compared to the Bare AuE (R_{ct} = 2.60x10^6 Ω), AuE/L-cysteine-In_3TeSe_2 QD (R_{ct} = 5.54x10^5 Ω), AuE/L-cysteine QD-EDC/NHS (R_{ct} = 1.27x10^6 Ω) and AuE/L-cysteine QD-EDC/NHS-Streptavidin (R_{ct} = 3.11x10^6 Ω) . These results obtained prove that the AuE/L-cysteine-In_3TeSe_2 QD (R_{ct} = 5.54x10^5 Ω) is more favourable than the bare AuE and the rest of the modified electrodes due to its low R_{ct} value, it also suggests a faster electron transfer thus showing a more conductive system than the rest. It also proves that the Aptamer is a less conductive material, since the incorporation of the Aptamer into the AuE/L-cysteine QD-EDC/NHS-Streptavidin system resulted in an increase in charge transfer resistance. The increase in charge transfer resistance could also be that the transfer of electrons from the electrolyte solution and Aptamer become very slow to reach the semiconductor QD at the electrode interface. This would support the phenomena that states; the higher the charge transfer resistance the slower the electron movement at the electrode interface. However when the blocking agent 6-Mercapto-1-hexanol (MCH) solution was incorporated into the system the charge transfer resistance decreased to R_{ct} = 3.11x10^6Ω.

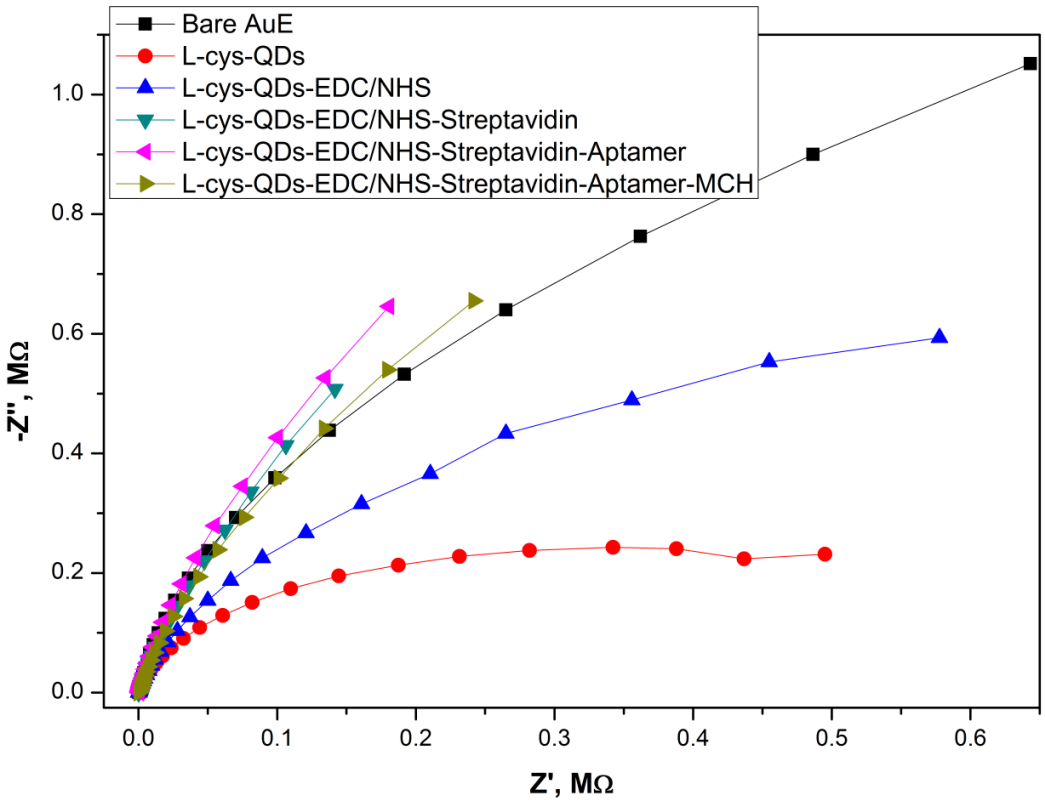

Figure 27: Nyquist plot at different steps of electrode fabrication in 0.1 M PBS, pH 7.4.

Table 1: Charge transfer resistance (R_{ct}) values for stepwise fabrication of QD based aptasensor.

Electrode System	R_{ct}, (Ω)	% Error
Bare AuE	2.60×10^6	2.05
AuE/L-Cysteine QD	5.54×10^5	1.31
AuE/L-Cys-QD-EDC/NHS	1.27×10^6	1.93
AuE/L-Cys-QD-EDC/NHS-Streptavidin	3.11×10^6	10.90
AuE/L-Cys-QD-EDC/NHS-Streptavidin-Aptamer	3.23×10^6	4.44
AuE/L-Cys-QD-EDC/NHS-Streptavidin-Aptamer-MCH	3.11×10^6	13.08

The Bode plot in **Figure 28** demonstrates the electrical properties of the materials. The phase angle for L-cysteine-In_3TeSe_2 (25.42˚) is less than that for bare AuE (58.63˚). However it gradually increases after each incubation step until the Aptamer is incorporated into the AuE/L-cysteine-In_3TeSe_2-EDC/NHS-Streptavidin system which then gave a phase angle of 74.37˚ less than the phase angle for AuE/L-cysteine-In_3TeSe_2-EDC/NHS-Streptavidin which was 74.40˚. These results indicate a decrease in conductivity of the AuE/L-cysteine-In_3TeSe_2-EDC/NHS-Streptavidin-Aptamer system because of the Aptamer. The phase angle then decreases further to 69.55˚ when the blocking agent; 6-Mercapto-1-hexanol (MCH) was introduced into the AuE/L-cysteine-In_3TeSe_2-EDC/NHS-Streptavidin-Aptamer system. However the AuE/L-cysteine QD-EDC/NHS-Streptavidin-Aptamer-MCH system is still conductive because it is still in the range of being conductive.

The total impedance, Z, data gave information on the conductive nature of the different systems. The log Z of bare AuE was 5.81 whereas the log Z for the AuE/L-cysteine-In_3TeSe_2 QD was 5.70. These results indicate that when the electrode systems were subjected to low frequency effects, the QD are more conducting than the gold electrode. At low frequency the log Z for AuE/L-cysteine-QD-EDC/NHS-Streptavidin-Aptamer was 5.25, meaning at this frequency this system is more conductive than the AuE/L-cysteine-In_3TeSe_2 QD system. However when the blocking agent MCH was incorporated into the AuE/L-cysteine-In_3TeSe_2 QD the log Z decreased to 5.39, thus the MCH is a less conducting material. The values obtained at each step of the QD aptasensor fabrication is displayed in **Table 2** below.

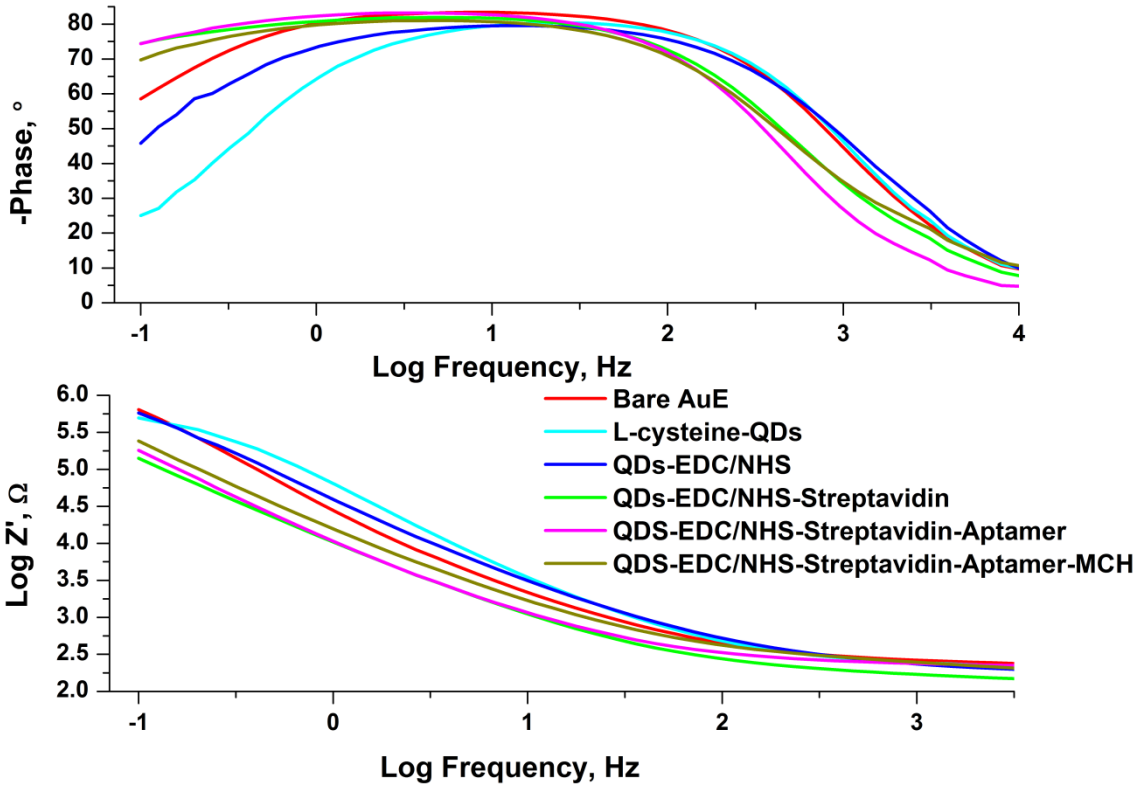

Figure 28: Bode plot at different steps of electrode fabrication in 0.1 M PBS, pH 7.4

Table 2: Phase angle and impedance values for the stepwise fabrication of the QD based aptasensor.

Electrode System	-Phase (˚)	Impedance
Bare AuE	58.63	5.81
AuE/L-Cysteine QD	25.42	5.70
AuE/L-Cys-QD-EDC/NHS	45.88	5.76
AuE/L-Cys-QD-EDC/NHS-Streptavidin	74.40	5.15
AuE/L-Cys-QD-EDC/NHS-Streptavidin-Aptamer	74.37	5.25
AuE/L-Cys-QD-EDC/NHS-Streptavidin-Aptamer-MCH	69.55	5.39

4.3. Aptasensor Measurements

4.3.1. Response parameters of L-cysteine-In_3TeSe_2 QD based aptasensor to Interferon-gamma (IFN-γ) using voltammetric techniques (CV, SWV).

In this study high sensitivity was achieved by interactions between the Aptamer molecule and the QD that was drop coated onto the AuE surface. The Aptamer probe was non-covalently tethered to the surface of the QD through a streptavidin-biotin reaction. The incorporation of the QD is advantages for the aptasensor under study since it relay an electrical signal that results from the binding of the aptamer and analyte .Mercapto Hexanol was used to prevent non-specific binding and to ensure that a high selectivity towards the target analyte is achieved. **Figure 29** shows the CV response obtained for the AuE/L-cysteine-In_3TeSe_2 QD/Aptamer to different concentrations (0.25-1.5 pg/mL) of IFN-γ in 0.1M PBS solution, pH 7.4. It can be seen that the oxidation peak potential at peak "A", which was used as the peak of interest decreases as different concentrations of the target IFN-γ was introduced, confirming the binding of the analyte to the aptamer at the electrode interface. The decrease in peak current is a result of the unfolding of the aptamer probe when it binds to the target analyte IFN- γ in 0.1M PBS solution, pH 7.4 (Huang, Tan, Shi, Liang, & Zhu, 2010). The decrease in peak current could also be due to the insulating properties of the aptamer that formed on the AuE surface. It is observed that as the IFN-γ concentration increases there is a shift in peak potentials, which is a characteristic of slow electron transfer kinetics in electrode reactions. Just like CV, SWV response was obtained for the L-cysteine-In_3TeSe_2 QD based aptasensor to different concentrations (0.25-1.5 pg/mL) of target IFN-γ in 0.1M PBS solution, pH 7.4 as displayed in **Figure 30.**

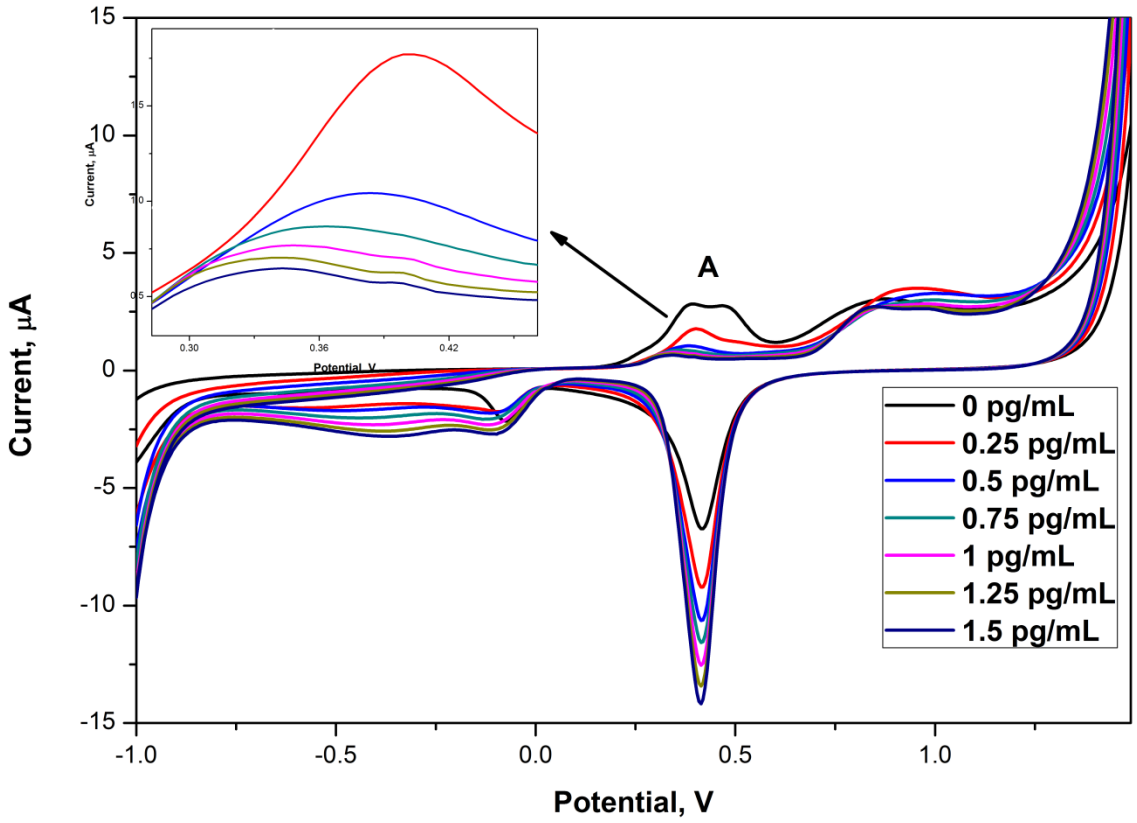

Figure 29: CV response of probe AuE/L-cysteine-In_3TeSe_2 QD/Aptamer to different concentrations of target IFN-γ in 0.1 M PBS, pH 7.4 at 0.04 V/s.

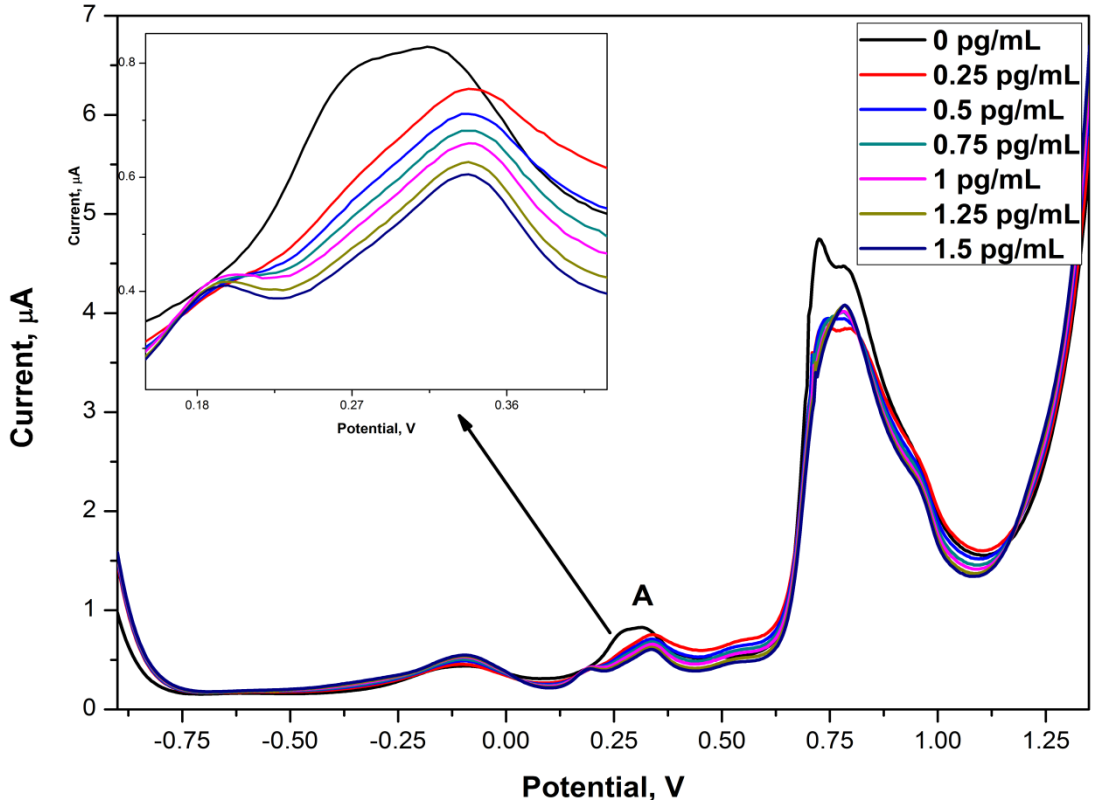

Figure 30: SWV response of probe AuE/L-cysteine-In_3TeSe_2 QD/Aptamer to different concentrations of target IFN-γ in 0.1 M PBS, pH 7.4 at 0.04 V/s.

The calibration curves that correspond to the CV and SWV responses are shown in **Figure 31** and **Figure 32**. Reader should bear in mind that only 4 concentrations was selected for CV and 5 concentrations for SWV calibration curves, since the dynamic linear range of the QD based aptasensor is within these concentrations. The CV current was linearly dependant on the concentration of IFN-γ in the range of 0.25-1 pg/mL with a linear correlation coefficient R^2= 0.99. The sensitivity was derived from the slope of the calibration curve which was 0.57 μA/(pg/mL) which is displayed in **Figure 31**. The SWV response showed a linear correlation coefficient R^2= 0.99 in the linear range 0.5-1.5 pg/mL with a corresponding sensitivity of 0.1 μA/(pg/mL) observed from the calibration curve in **Figure 32**.

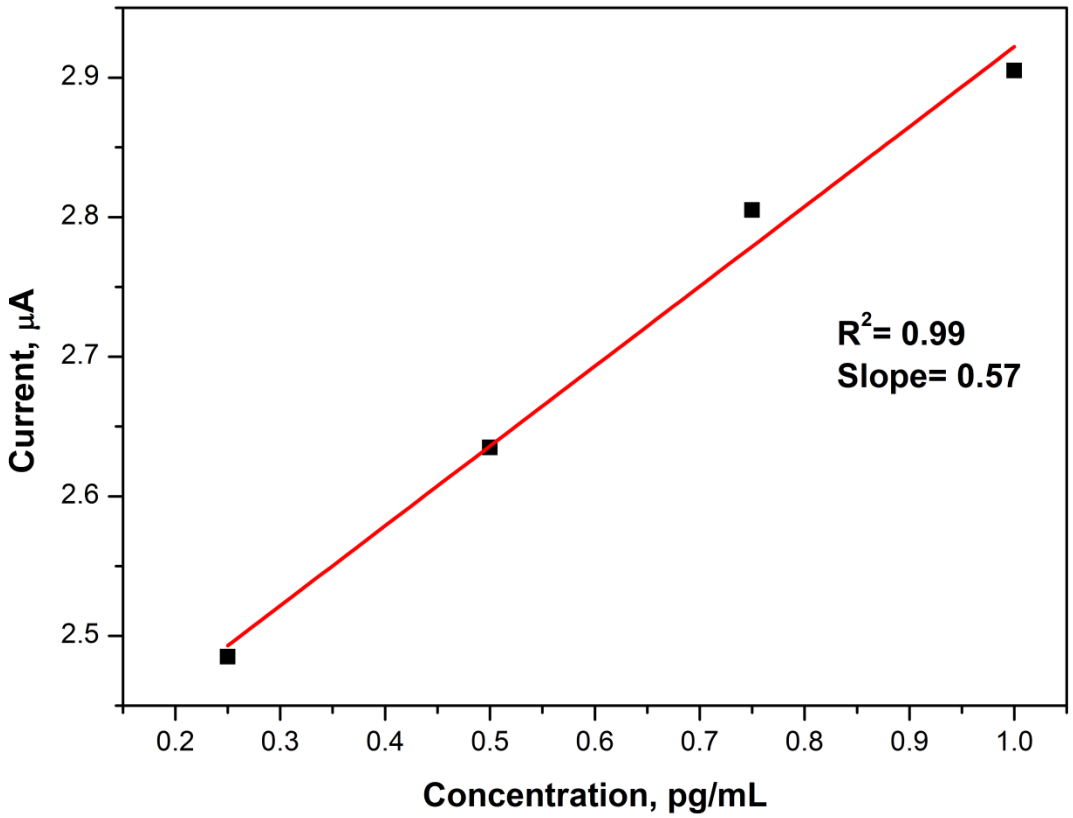

Figure 31: Calibration curve of the IFN-γ aptasensor (AuE/L-cysteine-In_3TeSe_2 QD/Aptamer) obtained from CV at 0.04 V/s in 0.1 M PBS, pH 7.4.

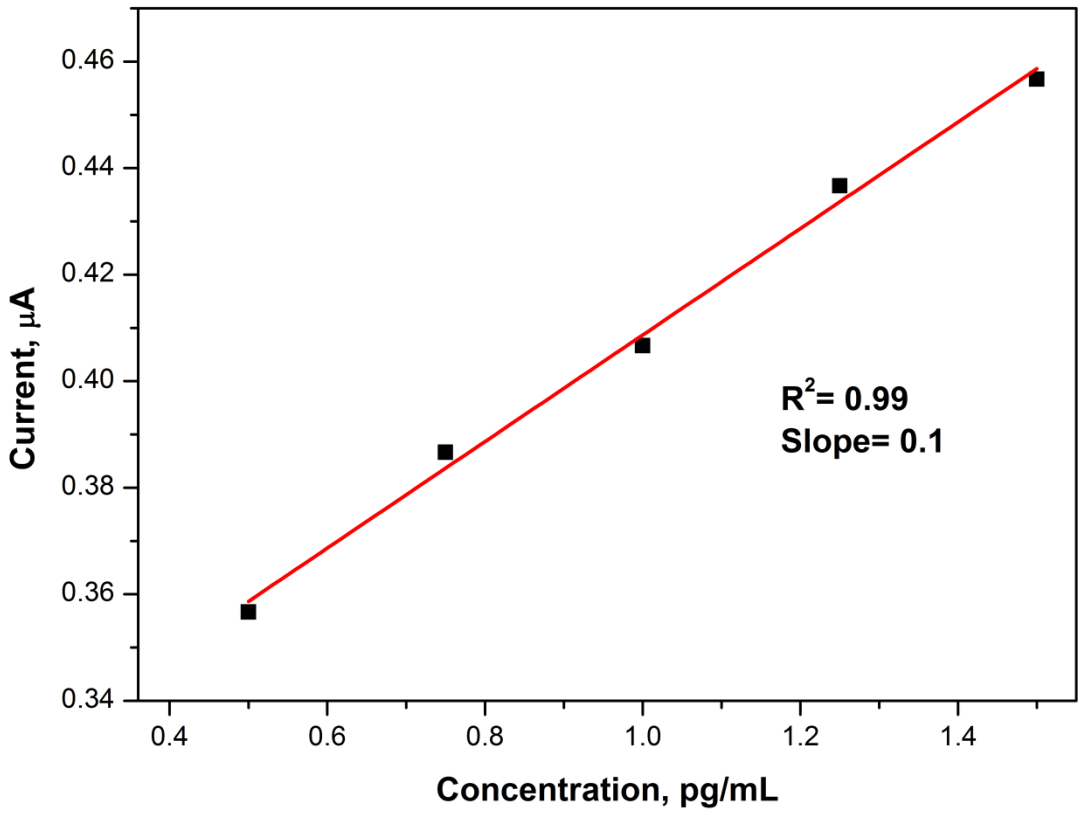

Figure 32: Calibration curve of the IFN-γ aptasensor (AuE/L-cysteine-In_3TeSe_2 QD/Aptamer) obtained from SWV at 0.04 V/s in 0.1 M PBS, pH 7.4.

4.3.2. Response parameters of L-cysteine-In_3TeSe_2 QD based aptasensor to Interferon-gamma (IFN-γ) using EIS.

The response of the probe AuE/L-cysteine-In_3TeSe_2 QD/Aptamer to different concentrations of target IFN-γ in PBS buffer solution, pH 7.4 was performed using EIS. The Nyquist plots were interpreted using Randles equivalent circuit displayed in **Figure 23** above. The Nyquist and Bode plot of the QD based aptasensor response to IFN-γ is shown in **Figure 33 (A)** and **(B)**. It is observed that the charge transfer resistance, phase angle and total impedance increased with increasing concentration of target analyte IFN-γ until it reached its saturation point at 1.5 pg/mL IFN-γ, this could be due to the decrease in current caused by IFN-γ. This behaviour suggests a slow electron transfer reaction.

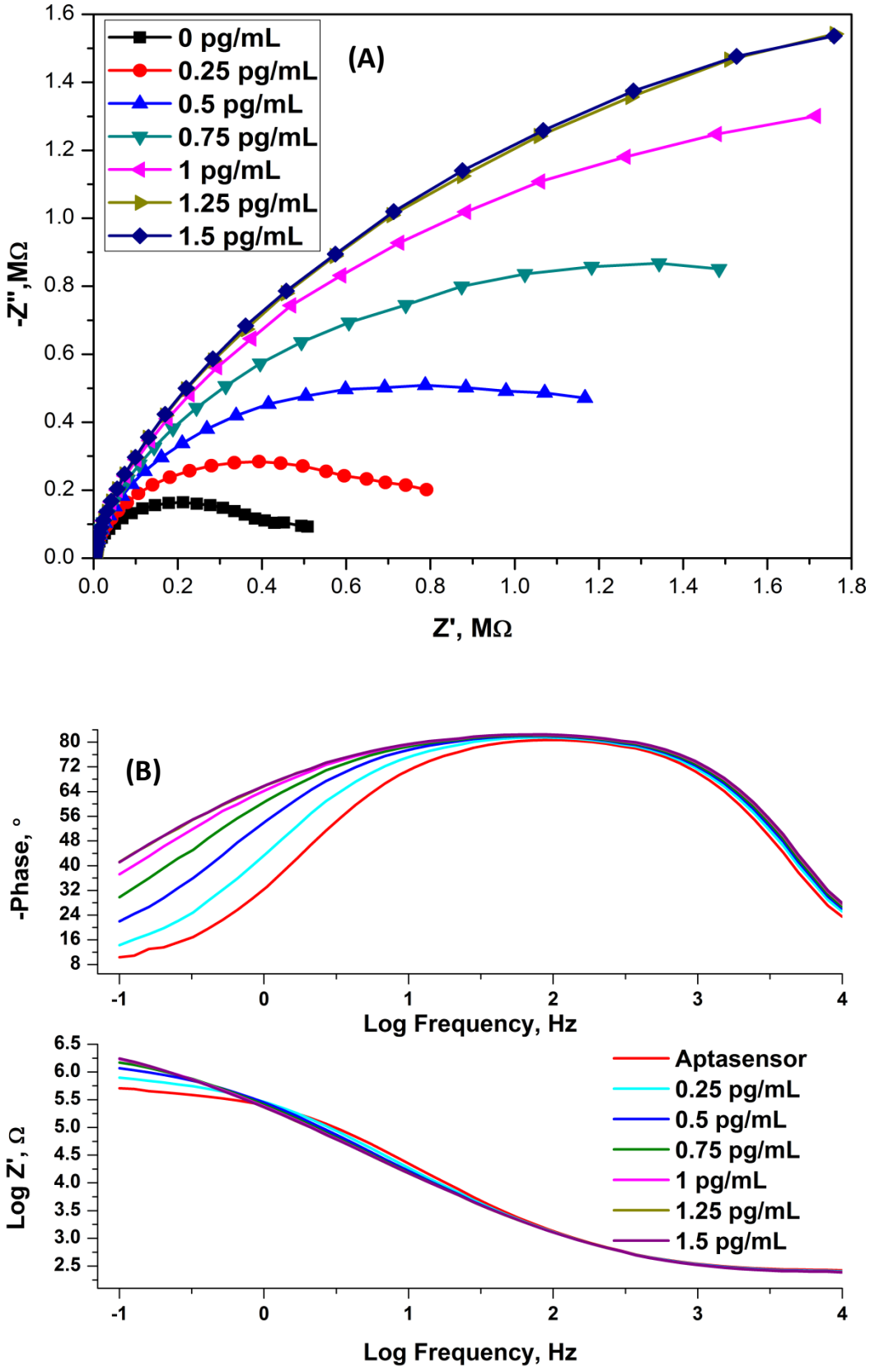

Figure 33: Nyquist plot (A) and Bode plot (B) of impedimetric response of probe AuE/L-cysteine-In_3TeSe_2 QD/Aptamer to different concentrations of IFN-γ in 0.1 M PBS, pH 7.4.

The calibration plots of charge transfer resistance (R_{ct}), total impedance and phase angle versus concentration of IFN-γ is displayed in **Figure 34**. The calibration plot based on the R_{ct} values in **Figure 34 (A)** shows a linear correlation coefficient of R^2 = 0.99 in the linear dynamic range of 0.25-1.25 pg/mL. The corresponding sensitivity was 2.25x10^6 Ω/(pg/mL). The calibration plot based on the total impedance values in **Figure 34 (B)**, shows a linear correlation coefficient of R^2 = 0.933 in the linear dynamic range of 0.25-1.0 pg/mL. The calibration plot based on the phase angle values in **Figure 34 (C)** displays a linear correlation coefficient of R^2 = 0.982 in the linear dynamic range of 0.25-1.25 pg/mL.

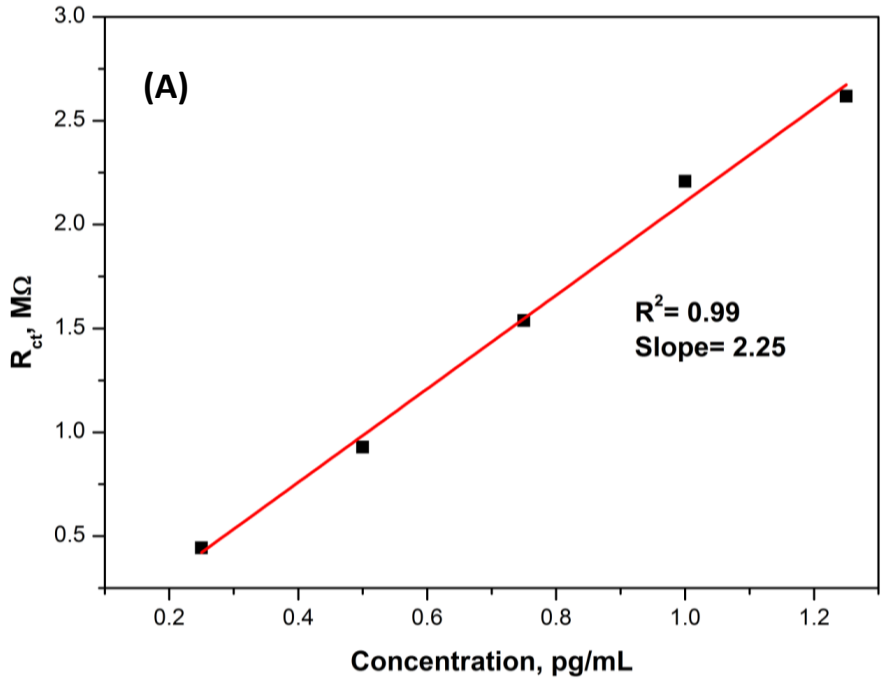

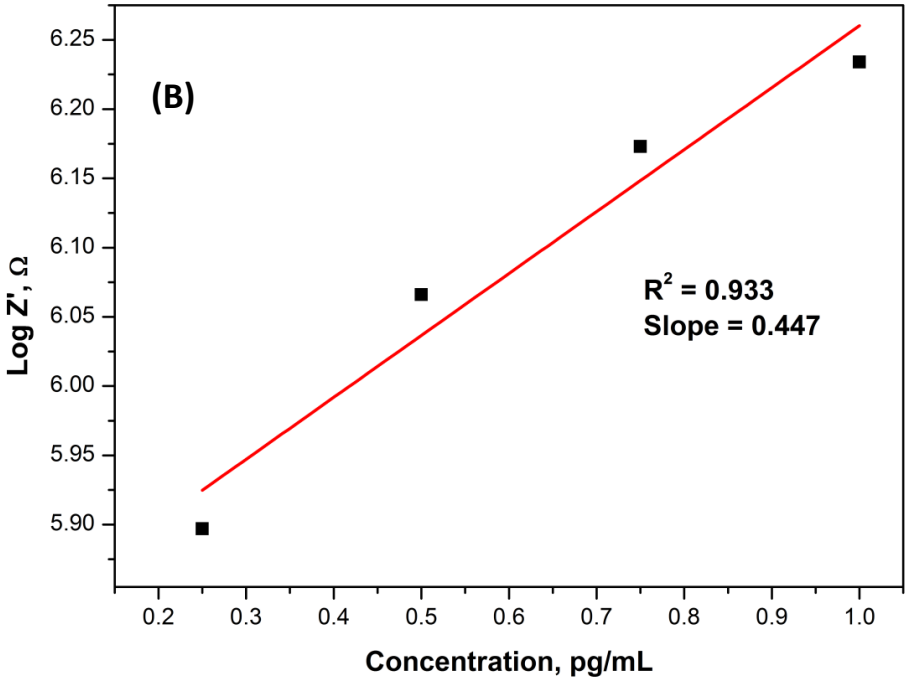

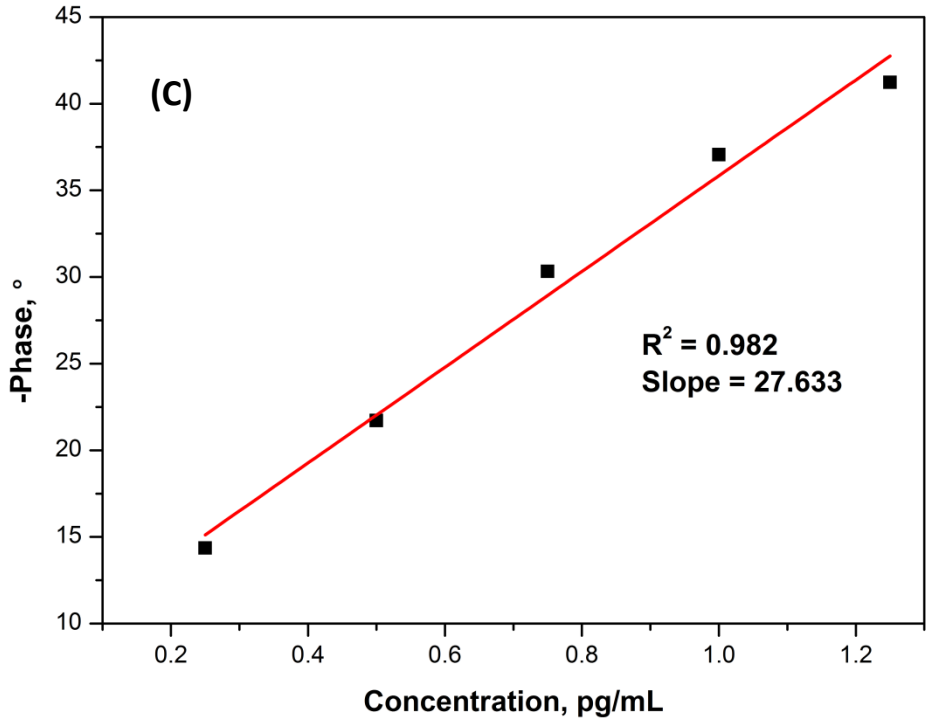

Figure 34: Calibration plot of the IFN-γ aptasensor (AuE/L-cysteine-In_3TeSe_2 QD/Aptamer based on R_{ct} (A), Total impedance (B) and Phase angle (C) values obtained from EIS in 0.1 M PBS, pH 7.4.

4.4. Comparison of analytical performance of the QD based Aptasensor using CV, SWV and EIS.

The L-cysteine-In_3TeSe_2 QD based Aptasensor response to different concentrations of target analyte IFN-γ was studied using CV, SWV and EIS. The performance of the L-cysteine-In_3TeSe_2 QD based Aptasensor using these three techniques were based on the dynamic linear range and sensitivity. The analytical parameters for these three techniques used (CV, SWV and EIS) was compared and described in **Table 3** below.

Table 3: Analytical performance of L-cysteine-InTeSe QD based aptasensor for CV, SWV and EIS techniques used.

Analytical Technique	Linear range (pg/mL)	Sensitivity in [μA/(pg/mL)]and [Ω/(pg/mL)]
CV	0.25-1	0.57
SWV	0.5-1.5	0.1
EIS	0.25-1.25	$2.25x10^6$

It is observed that all three analytical techniques used demonstrate good sensitivity and linearity since all three techniques shows a linear correlation coefficient of R^2= 0.99. It can be seen from the data in **Table 3** that EIS was the best technique to determine the performance of L-cysteine-In_3TeSe_2 QD based Aptasensor to different concentrations of IFN-γ. Using the EIS technique the L-cysteine-In_3TeSe_2 QD based Aptasensor showed a higher sensitivity ($2.25x10^6$ Ω/pg/mL) towards IFN-γ than both CV and SWV.

Liu and his colleagues developed an electrochemical DNA aptamer based biosensor to detect IFN-γ, there aptamer was thiolated and conjugated to methylene blue redox tag and immobilized onto the gold electrode by self-assembly. They used square wave voltammetry to detect IFN-γ. They had a linear range that went up to 10 nM and a sensitivity of 20 μA/(ng/mL) (Liu, Tuleouva, Ramanculov, & Revzin, 2010).

Xia and his colleagues developed a biosensor to detect interferon-gamma that was based on aptamer recognition and by the coupling of signal-on and signal-off modes. They used thiolated ferrocene and methylene blue as labels to hybridize interferon-gamma. They used square wave voltammetry to detect interferon-gamma and there biosensor had a linear range of 0.01-10 nM and sensitivity of 0.052 nM (Xia, et al., 2015).

Based on the biosensors mentioned in literature above, the novel L-cysteine-In_3TeSe_2 QD based aptasensor in this study is more sensitive to interferon-gamma and has a much better linear range. While the ELISA for interferon-gamma is more sensitive (Siawaya, et al., 2008), this QD based aptasensor described in this study offers fast detection, it is not expensive and it directly detects interferon-gamma without the need for multiple labels.

Chapter 5

Conclusion

For the first time the successful fabrication and implementation of sensitive L-cysteine-In_3TeSe_2 QD based Aptasensor for detection of Interferon-gamma (IFN-γ) TB biomarker has been reported. The QD based Aptasensor is a simple, inexpensive and easy to use aptasensor that is sensitive towards its target analyte. The L-cysteine-In_3TeSe_2 QD that's incorporated into the aptasensor was successfully synthesized via microwave irradiation. HRTEM and SAXS studies revealed the formation of spherical QD with an average diameter of 6 nm while the UV-Vis studies of the QD revealed an absorption peak in the ultra-violet region, confirming the formation of small sized QD. FTIR studies revealed that the In_3TeSe_2 QD was indeed capped with the surfactant; L-cysteine and that the quantum dot was water soluble because of the hydroxyl groups present in the spectrum. The carboxyl groups also present in the spectrum of the L-cysteine-In_3TeSe_2 QD conferred the hydrophilicity and stability of the alloyed quantum dot in aqueous systems, hence broadening their potential applications in biochemistry diagnostics.

The L-cysteine-In_3TeSe_2 QD exhibited interesting electro-catalytic properties which were useful for the fabrication of the QD based aptasensor for IFN-γ detection. Interferon-gamma was successfully detected using the probe AuE/L-cysteine-In_3TeSe_2 QD/Aptamer in PBS buffer solution, pH 7.4. Three analytical techniques (CV, SWV and EIS) were used to study the performance of the L-cysteine-In_3TeSe_2 QD based aptasensor towards different concentrations of target IFN-γ. It was observed that all three techniques showed good linearity with R^2 corresponding to 0.99, however it was perceived that EIS was the best technique for the detection of IFN-γ compared to CV and SWV since it showed a higher sensitivity (2.25 Ω/pg/mL) towards IFN-γ detection.

When the QD based aptasensor in this study was compared with those in literature particularly Liu et al., and Xia et al., it was demonstrated that the proposed aptasensor had a better linear range and sensitivity for interferon-gamma than both electrochemical sensors. The sensitivity of the QD based aptasensor in this study is still less than the traditional interferon-gamma ELISA, however it offers fast detection, is inexpensive and does not need multiple labelling as in ELISA. This novel QD based aptasensor can offer reliable information for Interferon-gamma diagnosis and promote the development of an effective and efficient evaluation of interferon-gamma. The goal of the developed QD based aptasensor is to apply it in real clinical samples of TB patients to detect interferon-gamma, TB biomarker.

Recommendations for future study

- Green nanotechnology should be used to synthesise the quantum dots.
- In depth research on novel nanomaterials that will increase the sensitivity of the aptasensors.
- Development of a simple, sensitive and reliable microfluidic device to detect IFN-γ to reach point of care device.
- It's suggested to make use of real clinical samples from TB patients instead of using IFN-γ standard solutions for the detections.
- Interferon-gamma should be detected using various detection methods (e.g., scanning electrochemical microscopy (SCEM), phase selective AC voltammetry (PSACV), electrochemiluminescence (ECL) and electrochemical quartz crystal microbalance (EQCM) to determine which detection method is the best for detecting interferon-gamma.

References

Acharya, T. (2012, April 10). *Microbe Online*. Retrieved November 29, 2016, from ELISA Test: Principle, Materials, Procedure and Results: https://microbeonline.com/elisa-test-for-antigenantibody-detection/

Alexeiv, U., & Farrens, D. (2014). Fluorescence spectroscopy of rhodopsins: Insights and approaches. *Biochimica et Biophysica Acta*, 694-709.

Baghar, A. M. (2016). Quantum Dots Applications. *Sensors and Transducers*, 37-43.

Bagner, A., Jouneau, P.-H., Thollet, G., Basset, D., & Gauthier, C. (2007). A history of scanning electron microscopy developments: Towards "wet-STEM" imaging. *Micron*, 390-401.

Bahadir, E. B., & Sezginturk, M. K. (2015). Applications of electrochemical immunosensors for early clinical diagnosis. *Talanta*, 162-174.

Bahadir, E. B., & Sezginturk, M. K. (2015). Applications of electrochemical immunosensors for early clinical diagnostics. *Talanta*, 162-174.

Chang, C.-c., Lin, S., Lee, C.-H., Chuang, T.-L., Hsueh, P.-r., Lai, H.-C., et al. (2012). Amplified surface plasmon resonance immunosensor for interferon-gamma based on streptavidin-incorporated aptamer. *Biosensors and Bioelectronics*, 68-74.

Chen, Y., Zou, C., Mastalerz, M., Hu, S., Gasaway, C., & Tao, X. (2015). Applications of Micro-Fourier Transform Infrared Spectroscopy (FTIR) in the Geological Sciences- A Review. *Molecular Sciences*, 30223-30250.

Choi, J., Chen, K. H., & Strano, M. S. (2006). Aptamer-capped nanocrystal quantum dots: A new method for label-free protein detection. *American Chemical Society*, 15584-15585.

Chung, Y., & Lee, C.-W. (2012). Electrochemical behaviours of Iindium. *Electrochemical Science and Technology*, 1-13.

Damborsky, P., Svital, J., & Katrilik, J. (2016). Optical biosensors. *Essays in Biochemistry*, 91-100.

Darsanaki, R. K., Azizzadeh, A., Nourbakhsh, M., Raeisi, G., & Aliabadi, M. A. (2013). Biosensors: Functions and Applications. *Biology and today's world*, 53-61.

Dey, D., & Goswami, T. (2011). Optical Biosensors: A revolution towards quantum nanoscale electronics device fabrication. *Biomedicine and Biotechnology*, 1-7.

Dogan-Topal, B., Ozkan, S., & Uslu, B. (2010). The analytical applications of square wave voltammetry on pharmaceutical analysis. *Open Chemical and Biomedical Methods*, 56-73.

Evans, D. H., O'Connell, K., Petersen, R. A., & Kelly, M. J. (1983). Cyclic Voltammetry. *Chemical Education*, 290-293.

Fan, X., White , I. M., Shopova, S. I., Zhu, H., Suter, J. D., & Sun, Y. (2008). Sensitive optical biosensors for unlabeled targets: A review. *Analytica Chimica Acta*, 8-26.

Fang, Z., Liu, L., Xu, L., Yin, X., & Zhong, X. (2008). Synthesis of highly stable dihydrolipoic acid capped water-soluble CdTe nanocrystals. *Nanotechnology*, 235603.

Farid, S., Meshik, X., Choi, M., Mukherjee, S., Lan, Y., Parikh, D., et al. (2015). Detection of Interferon gamma using graphene and aptamer based FET-like electrochemical biosensor. *Biosensor and Bioelectronics*, 294-299.

Fasmin, F., & Srinivasan, R. (2017). Review-Nonlinear electrochemical impedance spectroscopy. *Electrochemical Society*, 443-455.

Gan, S. D., & Patel, K. R. (2013). Enzyme Immunoassay and Enzyme-Linked Immunosorbent Assay. *Investigative Dermatology*, 1-3.

Gopinath, S. C., Tang, T.-H., Citartan, M., Chen, Y., & Lakshmipriya, T. (2014). Current aspects in immunosensors. *Biosensors and Bioelectronics*, 292-302.

Grieshaber, D., MacKenzie, R., Voras, J., & Reimhult, E. (2008). Electrochemical Biosensors- Sensor principles and architectures. *Sensors*, 1400-1458.

Grieshaber, D., MacKenzie, R., Voros, J., & Reimhult, E. (2008). Electrochemical Biosensors- Sensor Principles and Architectures. *Sensors*, 1400-1458.

Gullapalli, S., & Barron, A. (2010, June 12). *Characterization of Group 12-16 (II-VI) Semiconductor Nanoparticles by UV-visible Spectroscopy*. Retrieved January 1, 2018, from Connexions Web site: https://archive.cnx.org/contents/37d0488d-2a89-45db-b705-164961e44c50@1/characterization-of-group-12-16-ii-vi-semiconductor-nanoparticles-by-uv-visible-spectroscopy#eip-986

Harvey, D. (2017, January 18). *LibreTexts*. Retrieved October 15, 2017, from Voltammetric Methods: https://chem.libretexts.org/Textbook_Maps/Analytical_Chemistry_Textbook_Maps/Map%3A_Analytical_Chemistry_2.0_(Harvey)/11_Electrochemical_Methods/11.4%3A_Voltammetric_Methods

He, Z., & Mansfeld, F. (2009). Exploring the use of electrochemical impedance spectroscopy (EIS) in microbial fuel cell studies. *Energy and Environmental Science*, 215-219.

Helfrick, J., & Bottomly, L. (2009). Cyclic square wave voltammetry of single and consecutive reversible electron transfer reactions. *Analytical Chemistry*, 9041-9047.

Hettler, S., Dries, M., Zeelan, J., Oster, M., Schroder, R., & Gerthsen, D. (2016). High-resolution transmission electron microscopy with an electrostatic Zach phase plate. *New Journal of Physics*, 1-7.

Hoa, X., Kirk, A., & Tabrizian, M. (2007). Towards integrated and sensitive surface plasmon resonance biosensors: A review of recent progress. *Biosensors and Bioelectronics*, 151-160.

Huang, H., Li, J., Shi, S., Yan, Y., Zhang, M., Wang, P., et al. (2015). Detection of interferon-gamma for latent tuberculosis diagnosis using an immunosensor based on CdS quantum dots coupled to magnetic beads as labels. *Electrochemical Science*, 2580-2593.

Huang, H., Tan, Y., Shi, J., Liang, G., & Zhu, J.-J. (2010). DNA aptasensor for the detection of ATP based on quantum dots electrochemiluminescence. *Nanoscale*, 606-612.

Hussam, A. (2006). Voltammetry: Dynamic electrochemical techniques. *Analytical Chemistry*, 661-689.

Jayakumar, A., Trivedi, T., Sharma, D., Rebosura, M., & Murugesan, L. K. (2016, October 21). *ResearchGate.* Retrieved June 15, 2017, from Real Time Applications of Electrochemical Impedance Spectroscopy -A Technical Assessment: https://www.researchgate.net/publication/309352822_Real_Time_Applications_of_Electrochemical_Impedance_Spectroscopy_-A_Technical_Assessment

Jorcin, J., Orazem , M., Pebere, N., & Tribollet, B. (2006). Cpe analysis by local electrochemical impedance spectroscopy. *Electrochimica Acta* , 1473-1479.

Kapitonov, A., Stupak, A., Gaponenko, S., Petrov, E., Rogach, A., & Eychmuller, A. (1999). Luminescence properties of thiol stabilized CdTe nanocrystals. *Physical Chemistry B*, 10109-10113.

Kim, Y. S., Raston, N. H., & Gu, M. B. (2016). Aptamer-based nanobiosensors. *Biosensors and Bioelectronics*, 2-19.

Kokkinos, C., Economou, A., & Prodromidis, M. I. (2016). Critical survey of different architectures and transduction strategies. *Trends in Analytical Chemistry*, 88-105.

Koneswaran, M., & Narayanaswamy, R. (2009). L-Cysteine-capped ZnS quantum dots based fluorescence sensor for Cu ion. *Sensors and Actuators B*, 104-109.

Lee, C.-Y., Wu, K.-Y., Su, H.-L., Hung, H.-Y., & Hsieh, Y.-Z. (2013). Sensitive label-free electrochemical analysis of human IgE using an aptasensor with cDNA amplification. *Biosensors and Bioelectronics*, 133-138.

Li, L., Liao, L., Ding, Y., & Zeng, H. (2017). Dithizone-etched CdTe nanoparticles-based fluorescence sensor for the off-on detection of cadmium ion in aqueous media. *Royal Society of Chemistry*, 10361-10368.

Liu, F., Kang, S. H., Lee, Y.-I., Choa, Y.-h., Mulchandani, A., Myung, N., et al. (2010). Enzyme mediated synthesis of phytochelatin-capped CdS nanocrystals. *Applied Physics Letters*, 123703-123705.

Liu, G., & Lin, Y. (2007). Nanomaterial labels in electrochemical immunosensors and immunoassays. *Talanta*, 308-317.

Liu, P., Wang, Q., & Li, X. (2009). Studies on CdSe/L-cysteine Quantum Dots Synthesized in Aqueous Solution for Biological labeling. *Physical Chemistry C*, 7670-7676.

Liu, Q., Wang, J., & Boyd, J. B. (2015). Peptide-based biosensors. *Talanta*, 114-127.

Liu, Y., Tuleouva, N., Ramanculov, E., & Revzin, A. (2010). Aptamer-based electrochemical biosensor for interferon gamma detection . *Analytical Chemistry*, 8131-8136.

Macdonald, D. D. (2006). Reflections on the history of electrochemical impedance spectroscopy. *Electrochimica Acta*, 1376-1388.

Matos, C. R., Candido, L. P., Souza Jr, H. O., da Costa, L. P., Sussuchi, E. M., & Gimenez, I. F. (2016). Study of the aqueous synthesis, optical and electrochemical characterization of alloyed ZnxCd1-xTe nanocrystals. *Materials Chemistry and Physics*, 104-111.

Min, K., Cho, M., Han, S.-Y., Shim, Y.-B., Ku, J., & Ban, C. (2008). A simple and direct electrochemical detection of interferon-gamma using its RNA and DNA aptamers. *Biosensors and Bioelectronics*, 1819-1824.

Nicholson, R. (1965). Theory and Application of cyclic voltammetry for measurements of electrode reaction kinetics. *Analytical Chemistry*, 1351-1355.

Nurmalasari, R., Yohan, Gaffar, S., & Hartati, Y. W. (2015). Label-free electrochemical DNA biosensor for the detection of Mycobacterium tuberculosis using gold electrode modified by self-assembled monolayer of thiol. *Procedia Chemistry*, 111-117.

Ojeda, J. J., & Dittrich, M. (2012). Fourier transform infrared spectroscopy for molecular analysis of microbial cells. *Methods Mol Biol.*, 187-211.

Osteryoung, J. G., & Osteryoung, R. A. (1985). Square Wave Voltammetry. *Analytical Chemistry*, 101-110.

Pai, M., Denkinger, C. M., Kik, S. V., Rangaka, M. X., Zwerling, A., Oxlade, O., et al. (2014). Gamma Interferon Release Assays for detection of Mycobacterium Tuberculosis infection. *Clinical Microbiology Reviews*, 3-20.

Pai, M., Riley, L. W., & Colford Jr, J. M. (2004). Interferon-gamma assays in the immunodiagnosis of tuberculosis: a systematic review. *Infectious Diseases*, 761-776.

Parida, S., & Kaufmann, S. H. (2010). The quest for biomarkers in tuberculosis . *Discovery Today*, 148-157.

Patel, P., Mishra, V., & Mandloi, A. (2010). Biosensors: Fundamentals and Trends. *Engineering Research and Studies*, 15-34.

Pease, R., & Nixon, W. (1965). High resolution scanning electron microscopy. *SCI. Instrum*, 81-85.

Pena-Pereira, F., Costas-Mora, I., Romero, V., Lavilla, I., & Bendicho, C. (2011). Advances in miniaturzed UV-Vis spectrometric systems. *Trends in Analytical Chemistry*, 1637-1648.

Pereira, F., Vazquez, M., Deban, L., & Aller, A. (2013). Cyclic voltammetry of arsenic-doped cystein-capped ceramic nanoparticles. *Electrochimica Acta*, 125-135.

Pohanka, M., & Skladal, P. (2008). Electrochemical biosensors- principles and applications. *Applied Biomedicine*, 57-64.

Pokhrel, P. (2015, June 9). *Microbiology Notes*. Retrieved November 29, 2016, from ELISA-Principle, Types and Applications: http://www.microbiologynotes.com/elisa-principle-types-and-applications/

Rakesh Dhar, D. (2014). Synthesis and current applications of quantum dots. *Nanoscience and Nanotechnology*, 32-38.

Rogach, A., Franzl, T., Klar, T., Feldmann, J., Gaponik, N., Lesnyak, V., et al. (2007). Aqueous synthesis of thiol-capped CdTe nanocrystals: State of the Art. *Physical Chemistry C*, 14628-14637.

Schnablegger, H., & Singh, Y. (2011). *The SAXS guide: getting acquainted with the principles.* Graz, Austria: Austria: Anton Paar GmbH.

Shankaran, D. R., Gobi, K. V., & Miura, N. (2007). Recent advancements in surface plasmon resonance immunosensors for detection of small molecules of biomedical, food and environmental interest. *Sensors and Actuators B*, 158-177.

Siawaya, J. F., Roberts, T., Babb, C., Black, G., Golakai, J. H., Stanley, K., et al. (2008, July 2). *PLoS ONE.* Retrieved January 8, 2018, from National Centre for Biotechnology Information: https://www.ncbi.nlm.nih.gov/pmc/articles/PMC2432042/

Sipova, H., Sevcu, V., Kuchar, M., Ahmad, J. N., Mikulecky, P., Sebo, P., et al. (2011). Sensitive detection of interferon-gamma with engineered proteins and surface plasmon resonance biosensor. *Procedia Engineering*, 940-943.

Sipova, H., Sevcu, V., Kuchar, M., Ahmad, J., Mikulecky, P., Osicka, R., et al. (2012). Surface plasmon resonance biosensor based on engineered proteins for direct detection of interferon-gamma in diluted blood plasma. *Sensors and Actuators B*, 306-311.

Song , S., Wang, L., Li, J., Zhao, J., & Fan, C. (2008). Aptamer-based biosensors. *Trends in Analytical Chemistry*, 108-117.

Srivastava, S. K., van Rijn, C. J., & Jongsma, M. A. (2016). Biosensor- based detection of tuberculosis. *Royal Society of Chemistry*, 17759-17771.

Srivastava, S. K., van Rijn, C. J., & Jongsma, M. A. (2016). Biosensor-based detection of tuberculosis. *Royal Society of Chemistry*, 17759-17771.

Subramaniam, S. B. (2009). Interferon-gamma release assays (igras) for diagnosis of tuberculosis. *Pediatric Infectious Disease* , 33-37.

Suroviec, A. (2013). Introduction of Electrochemistry . *Laboratory Chemical Education*, 45-48.

Torati, S. R., Reddy, V., Yoon, S. S., & Kim, C. (2016). Electrochemical biosensor for Mycobacterium Tuberculosis DNA detection based on gold nanotubes array electrode platform. *Biosensors and Bioelectronics*, 483-488.

Torres-Chavolla, E., & Alocilja, E. C. (2011). Nanoparticle based DNA biosensor for tuberculosis detection using thermophilic helicase-dependent isothermal amplification. *Biosensors and Bioelectronics*, 4614-4618.

Tuleuova, N., Jones, C. N., Yan, J., Ramanculov, E., Yokobayashi, Y., & Revzin, A. (2010). Development of an aptamer beacon for detection of interferon-gamma. *Analytical Chemistry*, 1851-1857.

von Aulock, F., Kennedy, B., Schipper, C., Castro, J., Martin, D., Oze, C., et al. (2014). Advances in Fourier transform spectroscopy of natural glasses: From sample preparation to data analysis. *Lithos*, 52-64.

Wang, J. (2006). Electrochemical biosensors: Towards point-of-care cancer diagnostics. *Biosensors and Bioelectronics*, 1887-1892.

Wang, Q., Moser, J., & Gratzel, M. (2005). Electrochemical impedance spectroscopic analysis of dye-sensitized solar cells. *Physical Chemistry B*, 14945-14953.

Wang, Y., Hu, R., Lin, G., Roy, I., & Yong, K.-T. (2013). Functionalized quantum dots for biosensing and bioimaging and concerns on toxicity. *ACS Applied Materials Interfaces*, 2786-2799.

Wang, Z. (2000). Transmission Electron Microscopy of shape-controlled nanocrystals and their assemblies. *Phys Chem B*, 1153-1175.

Wen, W., Yan, X., Zhu, C., Du, D., & Lin, Y. (2017). Recent advances in electrochemical immunsensors. *Analytical Chemistry*, 138-156.

Wijaya, E., Lenaerts, C., Maricot, S., Hastanin, J., Habraken, S., Vilcot, J.-P., et al. (2011). Surface plasmon resonance-based biosensors: from the development of different SPR structures to novel surface functionalization strategies. *Current opinion in solid state and material science*, 208-224.

Winterflood, C. M., Ruckstuhl, T., & Seeger, S. (2013). Fast and sensitive interferon-gamma assay using supercritical angle fluorescence. *Biosensors*, 108-115.

Wood, R. (1902). On a remarkable case of uneven distribution of light in a diffraction grating spectrum. *Phil Mag*, 396-402.

Xia, J., Song, D., Wang, Z., Zhang, F., Yang, M., Gui, R., et al. (2015). Single electrode biosensor for simultaneous determination of interferon gamma and lysozyme. *Biosensors and Bioelectronics*, 55-61.

Xia, X., Zun-zhong, Y., Jian, W., & Yi-bin, Y. (2010). Application and research development of surface plasmon resonance-based immunosensors for protein detection. *Chinese Journal of Analytical Chemistry*, 1052-1059.

Yan , G., Wang, Y., He, X., Wang, K., Liu, J., & Du, Y. (2013). A highly sensitive label-free electrochemical aptasensor for interferon-gamma detection based on graphene controlled assembly and nuclease cleavage-assisted target recycling amplification. *Biosensors and Bioelectronics*, 57-63.

Yang, F., Yang, P., & Cao, Y. (2013). Hydrothermal synthesis of high-quality thiol-stabilized CdTeSe alloyed quantum dots . *Fluoresc*, 1247-1254.

Yang, Z., Jian, Z., Chen, X., Li, J., Qin, P., Zhao, J., et al. (2015). Electrochemical impedance immunosensor for sub-picogram level detection of bovine interferon-gamma based on cylinder-shaped Tin dioxide nanorods. *Biosensors and Bioelectronics* , 190-195.

Zumla, A., Raviglione, M., Hafner, R., & Fordham van Reyn, C. (2013). Tuberculosis. *New England Journal of Medicine*, 745-755.